Circadian Rhythms and Diurnal Profiles of Salivary Alpha Amylase in Women with Breast Cancer

Christy Albert, BS[1], Trevor Stantliff[1], Elizabeth Cash, PhD[1,2,3], and Sandra E. Sephton, PhD[1,2]

[1]Department of Psychological and Brain Sciences, University of Louisville, Louisville, KY   [2]James Graham Brown Cancer Center, University of Louisville, Louisville, KY

[3]Department of Otolaryngology-HNS & Communicative Disorders, University of Louisville School of Medicine, Louisville, KY

Introduction

PURPOSE:
This study aims to examine the relationship between circadian activity rhythms and the diurnal profile of salivary alpha amylase in pre-surgical breast cancer women.

BACKGROUND:
Approximately 1 in 8 U.S. women will develop an invasive breast tumor during the course of her life. Numerous biological processes, including those responsible for tumor suppression, are organized into a hierarchy of phase coupled genetic oscillators incorporating auto-regulatory transcription-translation feedback loops. *Disruptions in this hierarchy result in tumor promoting environments[1].*

The suprachiasmatic nucleus (SCN), at the top of the hierarchy, follows an endogenous 24 hour cycle syncing itself to light/dark via photic information from the retina. Additionally, efferent and afferent pathways to many brain regions results in phase locking of downstream oscillators, regulating not only biological rhythms but also behavioral circadian rhythms such as the sleep/wake cycle and rest/activity rhythms**.** *Disruptions in these behavioral rhythms have associations with biomarkers of tumor progression[2].*

The diurnal profile of cortisol secretion, its connection to rest/activity rhythms[3], and cortisol's ability to reach peripheral organs suggests the HPA axis as a potential communicator between the SCN, diverse brain regions, and peripheral cell oscillators. Moreover, *disruptions of HPA rhythms, which can be caused by chronic stress, are prognostic for early mortality in breast cancer patients[4].*

The sympathetic nervous-adrenomedullary (SAM) system is also activated in response to stress and has the ability to signal peripheral organs. The SAM may be another mechanism by which the SCN coordinataes peripheral cell oscillators. Salivary alpha amylase (sAA), a biomarker for norepinephrine release via the SAM system, follows a diurnal profile.

Our laboratory's model (Figure 1) illustrates circadian effects in psychoneuroendocrine and immune pathways related to tumor progression (Eismann, et al., 2010). Circadian rhythms and autonomic activity influence tumor progression directly (pathways B and E) and/or indirectly (multiple pathways). This study investigates how they may influence (relationships to) each other (pathway A).
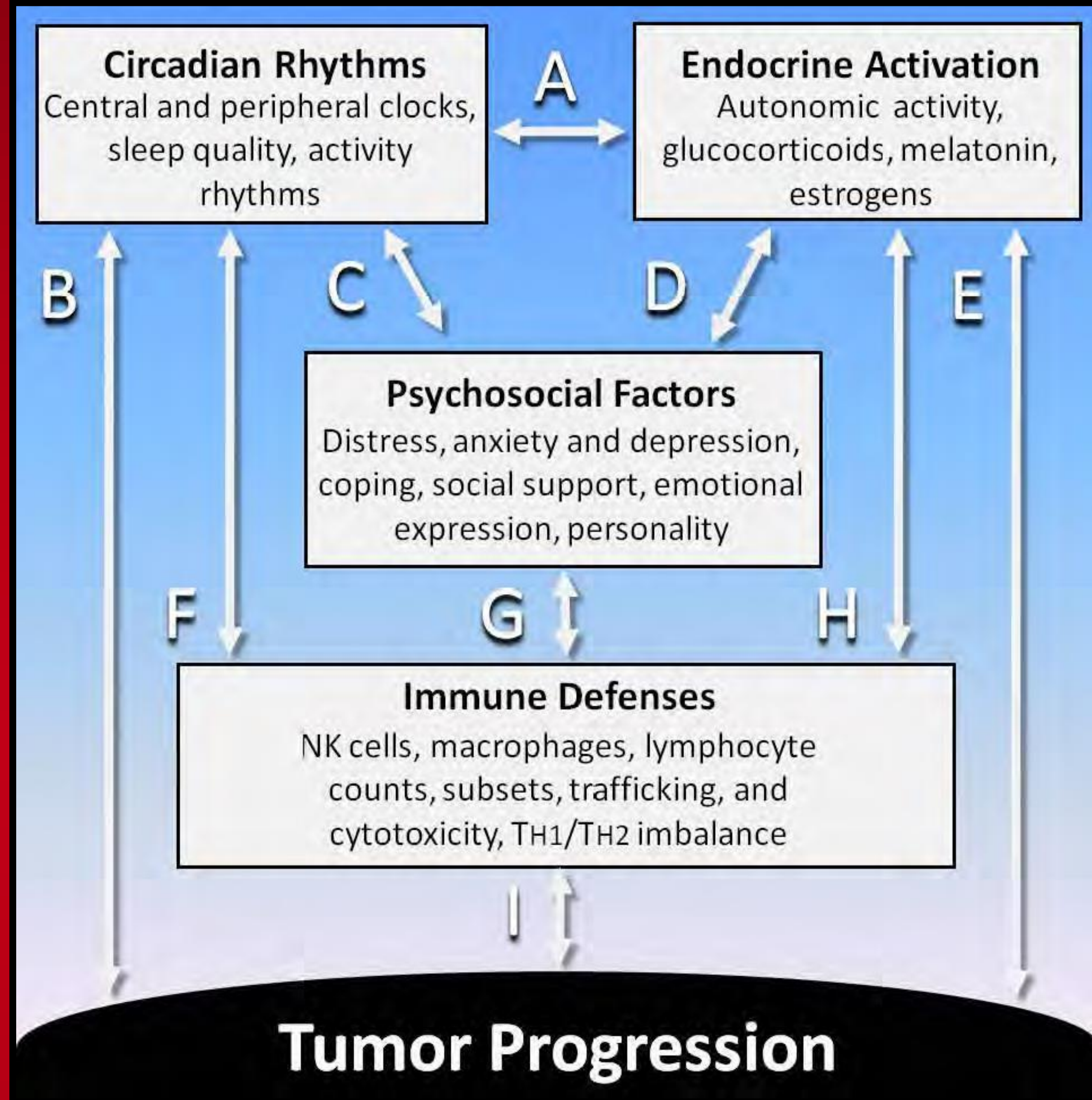
RATIONALE:
The non-invasive collection nature of sAA makes it a good candidate for studying the relationship between circadian activity rhythms and sympathetic activation in cancer patients.

While research investigating the HPA axis with regard to circadian activity rhythms has led to effective interventions ameliorating the effects of chronic stress on tumor progressions and cancer outcomes, research into sympathetic activation with regard to circadian regulation has been lacking.

Research here could shed new light on the mechanisms integrating biorhythms and behavior, resulting in more integrative approaches to cancer treatment.

Our laboratory's model of circadian effects in psychoneuroendocrine and immune pathways related to tumor progression (Eismann, et al., 2010)

Circadian Rhythms — Central and peripheral clocks, sleep quality, activity rhythms

Endocrine Activation — Autonomic activity, glucocorticoids, melatonin, estrogens

Psychosocial Factors — Distress, anxiety and depression, coping, social support, emotional expression, personality

Immune Defenses — NK cells, macrophages, lymphocyte counts, subsets, trafficking, and cytotoxicity, TH1/TH2 imbalance

Tumor Progression

Sample (N = 50)

Mean sAA levels in our group exhibit a diurnal profile with a dip in concentration 30 minutes after waking, a steady increase during the day, and a dip in concentration from 4pm to bed.

24 Hour Autocorrelation Coefficient Distribution

N	Valid	47
Mean		.279
Std. Deviation		.158
Range		.738
Minimum		-.074
Maximum		.721
Variance		.025

Actigraphy watches measure activity levels in one minute epochs. Auto-correlation is a technique used to show how one minute epochs on day 1 correlate with one minute epochs on subsequent days. Higher values are representative of stronger daily rhythms[5].
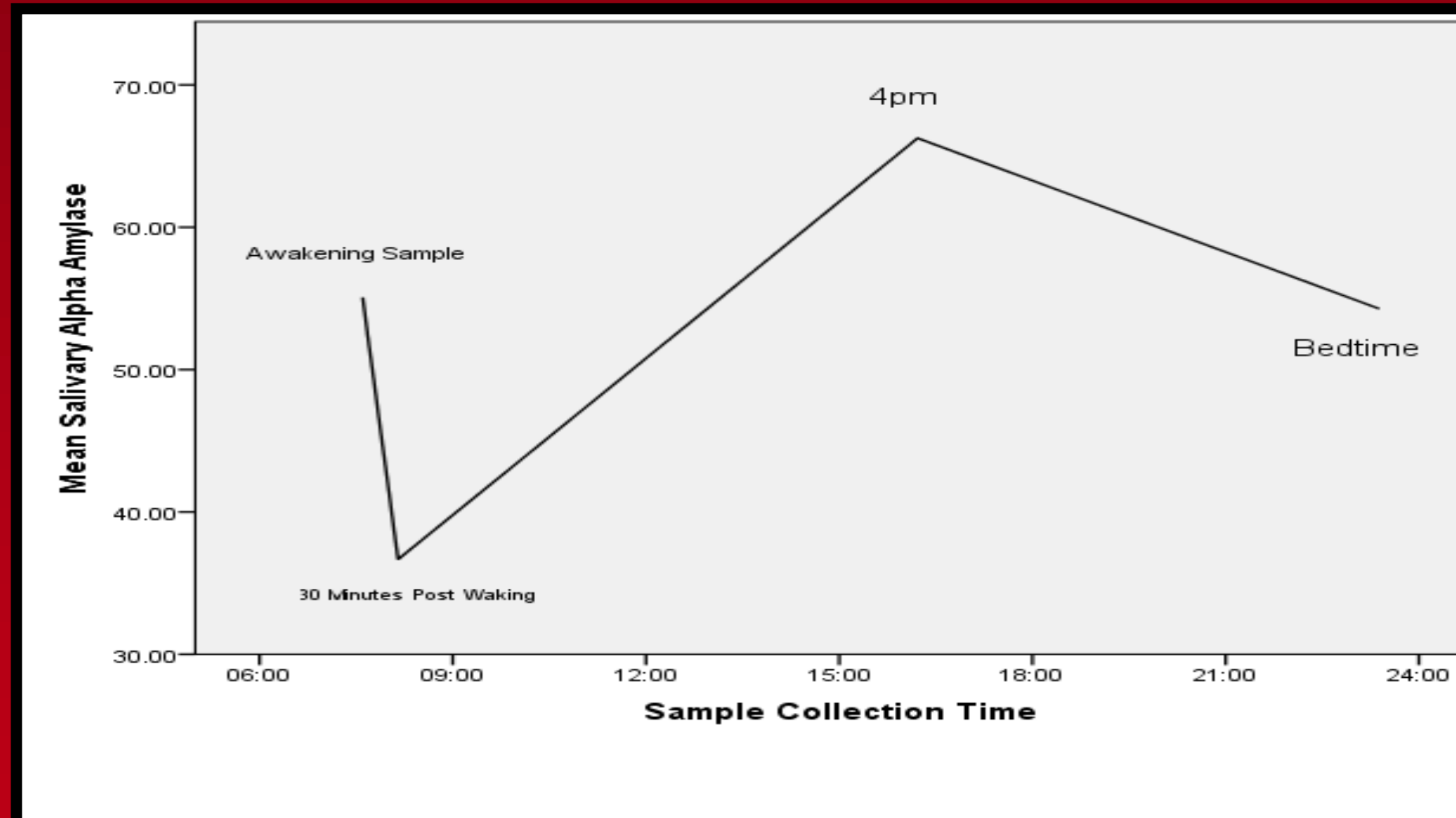

Methods

This study falls within the scope of a larger study in which sixty breast cancer patients awaiting surgery were recruited. None of the recruits were currently taking contraceptives or hormone replacement therapy. Saliva samples were collected from participants at awakening, 30 minutes post waking, 4pm, and bedtime over a collection period of three days. Participants also wore an actigraphy watch (ambulatory monitoring) during the collection period.

Salivary alpha amylase samples were quantified using kinetic assay technique (Salimetrics) which employs a 2-chloro-*p*-nitrophenol substrate linked to maltrose. Enzymatic activity of alpha amylase on this substrate yields 2-chloro-*p*-nitrophenol which can be spectrophotometrically measured at 405nm using a standard optical density plate reader. Raw amylase values were log transformed before slopes (waking to 30 minutes post waking; waking, 4pm, and bed; and 30 minutes post waking to 4pm) were calculated.

Actigraphy data was translated into rest/activity rhythm variables (24hr autocorrelation coefficient) using Action 4 software.

One participant was excluded due to shift work. Additional variances in N value reflect insufficient quantity of saliva samples (samples were first analysed for salivary cortisol), samples with collection times outside the proposed times, or other collection errors that invalidated the sample.

Results

Hierarchical linear regression models showed no significance (p>.05) between circadian activity rhythms (autocorrelation coefficient) and salivary alpha amylase diurnal profile slopes (waking, 4pm, and bed; waking to 4pm; post waking, 4pm, and bed; post waking to 4pm; and waking to 30 minutes post waking (morning response).

After controlling for age, stage, and income; models with circadian activity rhythms as a predictor showed no significance (p>.05) while models with amylase slope as a predictor became significant, with income as the only significant predictor to these models. Models with slope (Waking, 4pm, bed) as a predictor became significant (p=.02,R^2=.277) with income as the significant predictor to the model (p=.001,β=.511), models with amylase slope (waking to 4pm) became significant (p=.005, R^2=.346) with income as the significant predictor to the model (p=.001,β=.50), models with amylase slope (post waking, 4pm, bed) became significant (p=.022,R^2=.272) with income as the significant predictor to the model (p=.001,β=.51), models with amylase slope (post waking to 4pm) became significant (p=.021,R^2=.283) with income as the significant predictor to the model (p=.001,β=.52) and models with amylase slope (morning response) as a predictor became significant (p=.025,R^2=.272) with income as a significant predictor to the model (p=.002,β=.50)

Conclusions

Our study found no significance between circadian activity rhythms and the diurnal profile of salivary alpha amylase in this sample. However, significant relationships between circadian activity rhythms and the diurnal profile of cortisol were found from this same sample[3].

This may indicate that the oscillatory phase coupling mechanisms resulting in diurnal patterns of sympathetic activation are more robust against behavioral influences and exogenous signals compared to the HPA axis, or it could point to other mediators influencing the interplay between circadian activity rhythms and SNS activation. Additional research investigating these possible mediators could shed new light on this intricate interplay of biorhythms and behavior, leading to more integrative approaches to cancer treatment.

Additionally, income as a predictor reveals potential moderating effects of socioeconomic factors in these outcome variables, and illustrates the need for future studies to frame cancer research within a socioeconomic context.

Acknowledgements

References:
1. Fu, L., & Lee, C. C. (2003). The circadian clock: pacemaker and tumour suppressor. Nature Reviews Cancer, 3(5), 350-361.
2. Eismann, E. A., Lush, E., & Sephton, S. E. (2010). Circadian effects in cancer-relevant psychoneuroendocrine and immune pathways. Psychoneuroendocrinology, 35(7), 963-976.
3. Dedert, E., Lush, E., Chagpar, A., Dhabhar, F. S., Segerstrom, S. C., Spiegel, D., ... & Sephton, S. E. (2012). Stress, coping, and circadian disruption among women awaiting breast cancer surgery. Annals of behavioral medicine, 44(1), 10-20.
4. Sephton, S. E., Sapolsky, R. M., Kraemer, H. C., & Spiegel, D. (2000). Diurnal cortisol rhythm as a predictor of breast cancer survival. Journal of the National Cancer Institute, 92(12), 994-1000.
5. Ancoli-Israel, S., Cole, R., Alessi, C., Chambers, M., Moorcroft, W., & Pollak, C. (2003). The role of actigraphy in the study of sleep and circadian rhythms. American Academy of Sleep Medicine Review Paper. Sleep, 26(3), 342-392.

Optimizing IHC for Cisplatin Treated Tissue

Marisa Bohn and Levi J. Beverly
Department of Medicine, James Graham Brown Cancer Center
University of Louisville, Louisville, KY 40202, USA.

Abstract

Cisplatin is a platinum-based chemotherapeutic drug used today for the treatment of many different types of cancer. Although cisplatin is successful initially, its efficacy is impeded by the development of resistance during treatment. Many factors contribute to this development of resistance, such as the DNA repair mechanisms of damaged cells. Identification of specific proteins that contribute to these unique DNA repair pathways of cisplatin treated tissue may lead to the development of rational novel therapies for cisplatin resistant cancer. Immunohistochemistry has become an indispensable technique in understanding the histopathology of cisplatin treated tissues, identifying proteins and noting the differences between their levels of expression in cisplatin treated tissues vs. non-treated tissues can offer insight into the pathological mechanisms of cisplatin and potentially improve current chemotherapeutic strategies.
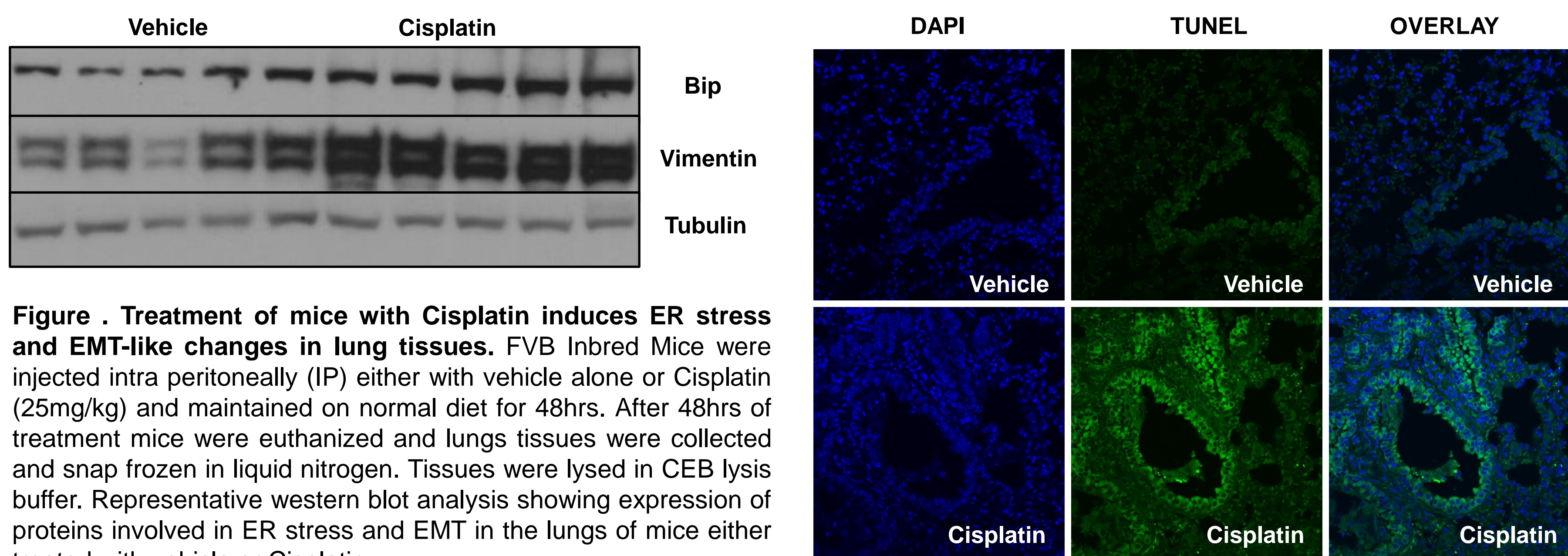
Results

Figure. Treatment of mice with Cisplatin induces ER stress and EMT-like changes in lung tissues. FVB Inbred Mice were injected intra peritoneally (IP) either with vehicle alone or Cisplatin (25mg/kg) and maintained on normal diet for 48hrs. After 48hrs of treatment mice were euthanized and lungs tissues were collected and snap frozen in liquid nitrogen. Tissues were lysed in CEB lysis buffer. Representative western blot analysis showing expression of proteins involved in ER stress and EMT in the lungs of mice either treated with vehicle or Cisplatin.
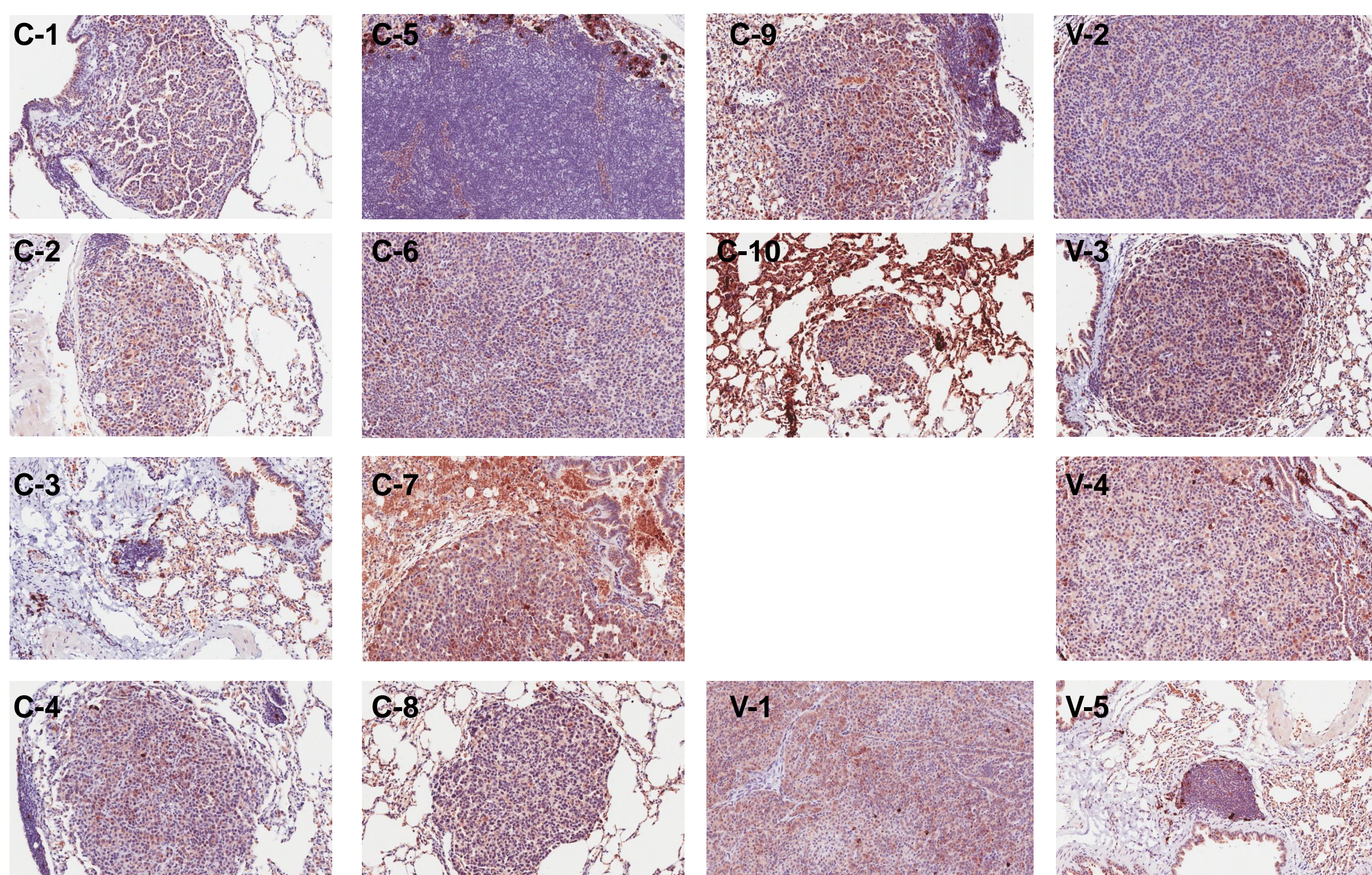
Figure. TUNEL staining for apoptosis using green fluorescent antibody
In Situ Cell Death Detection Kit was used for detection of apoptosis at single cell level of DNA strand breaks and then analyzed using confocal microscopy. The difference between the Vehicle and Cisplatin treated mice appear to be significantly different upon examination and suggest that Cisplatin induces programmed cell death.

Figure. Immunohistochemistry done on lung tissues of Cisplatin treated mice using ER stress marker Bip.
Bip is a protein chaperone and known biomarker of ER stress. When protein folding in the ER becomes disrupted, Bip synthesis increases. Cisplatin has been shown to induce ER stress causing a significant increase in Bip levels, indicating ER stress.
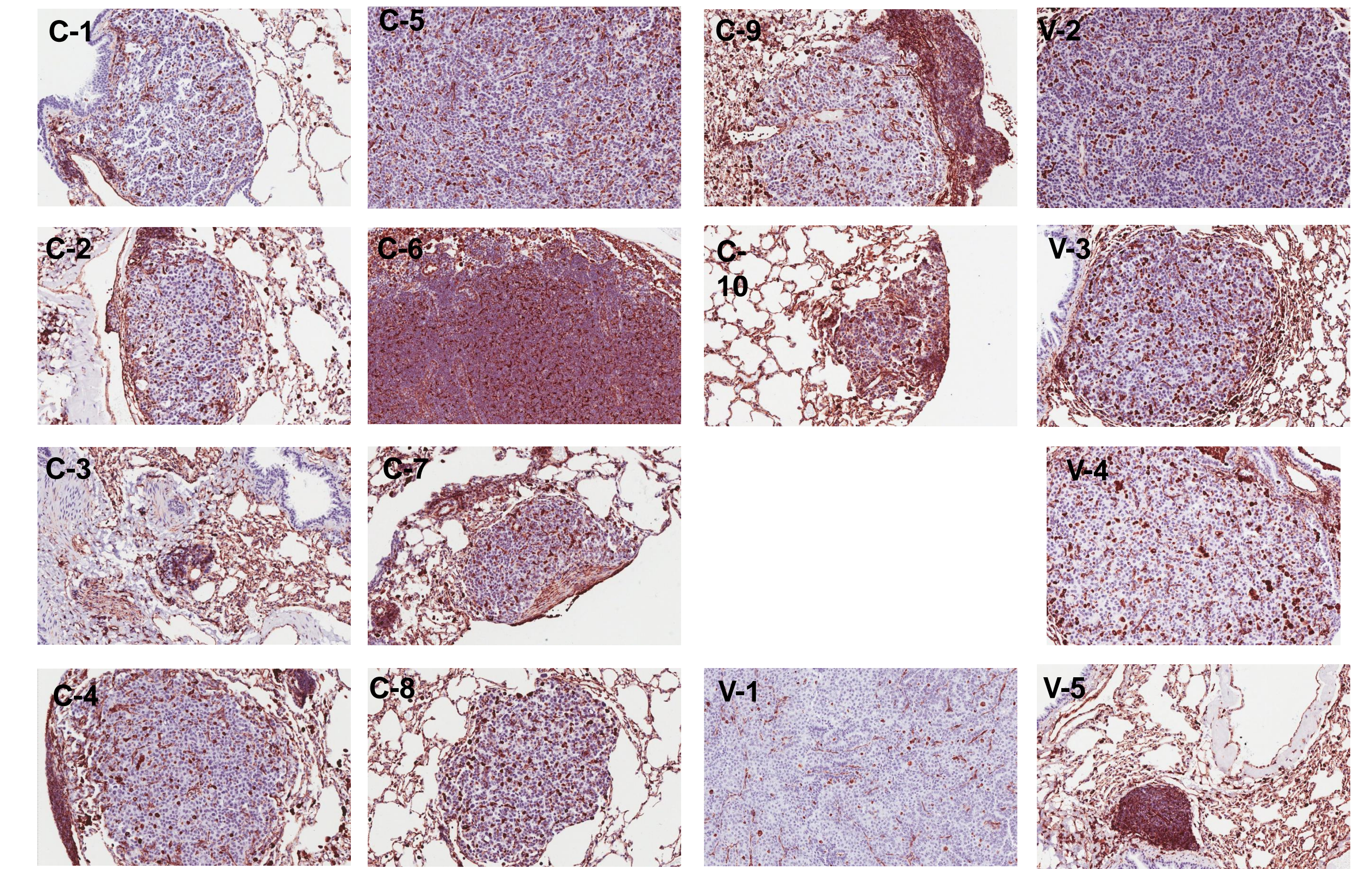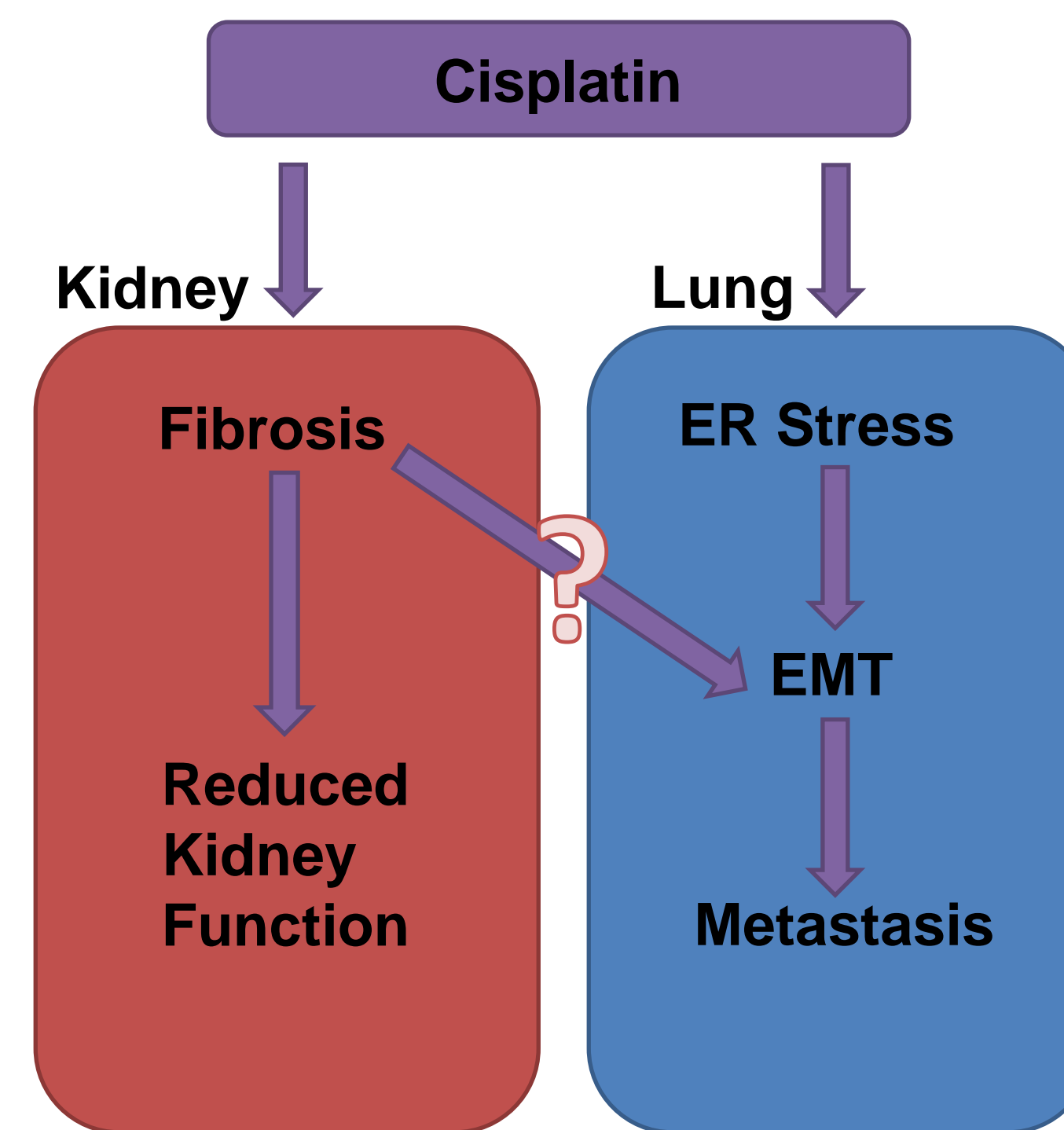

Figure. Immunohistochemistry done on lung tissues of Cisplatin treated mice using EMT marker Vimentin.
Vimentin is biomarker of EMT that has been shown to increase following treatment of Cisplatin. IHC was done on cisplatin treated and non-cisplatin treated tissues to examine the cells in which Vimentin is present.
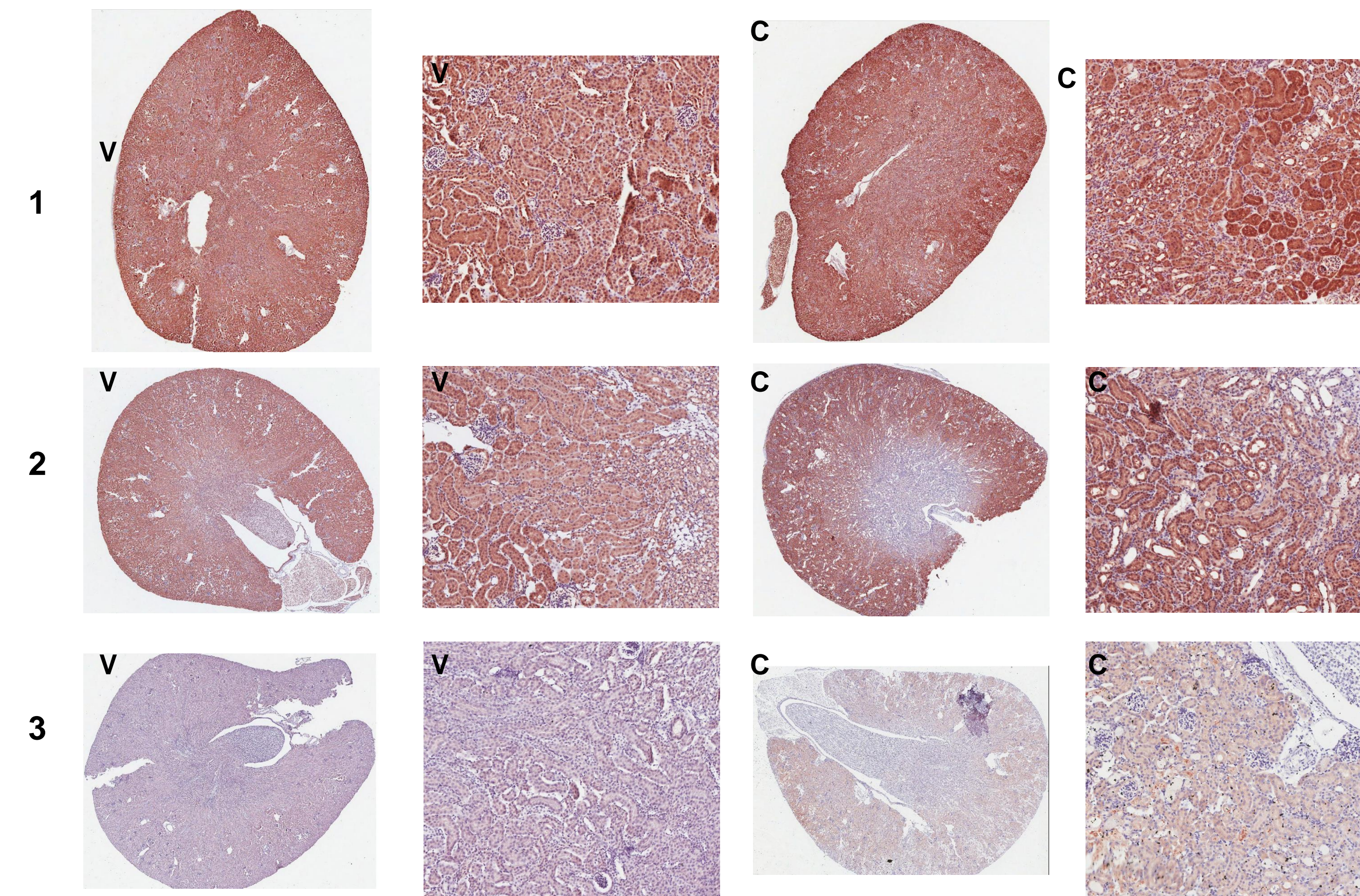
Figure. Immunohistochemistry on kidney tissues using Pai-1 antibody.
Pai-1 is biomarker for fibrosis which is has been shown to increase following treatment with Cisplatin. IHC was done to examine the cells Pai-1 was found in, however, reliable results failed to be produced. 3 Trials were done with alterations made to the protocol each time.

Conclusion

Optimization of protocols for TUNEL and Pai-1 in order to get reliable immunohistochemistry test results

Acknowledgements

Intra-operative Navigation of a 3-D Needle Localization for Precision of Irreversible Electroporation Needles in Locally Advanced Pancreatic Cancer

Logan Bond, Robert CG Martin II, MD, PhD

Department of Surgery, Division of Surgical Oncology, University of Louisville, Louisville, KY
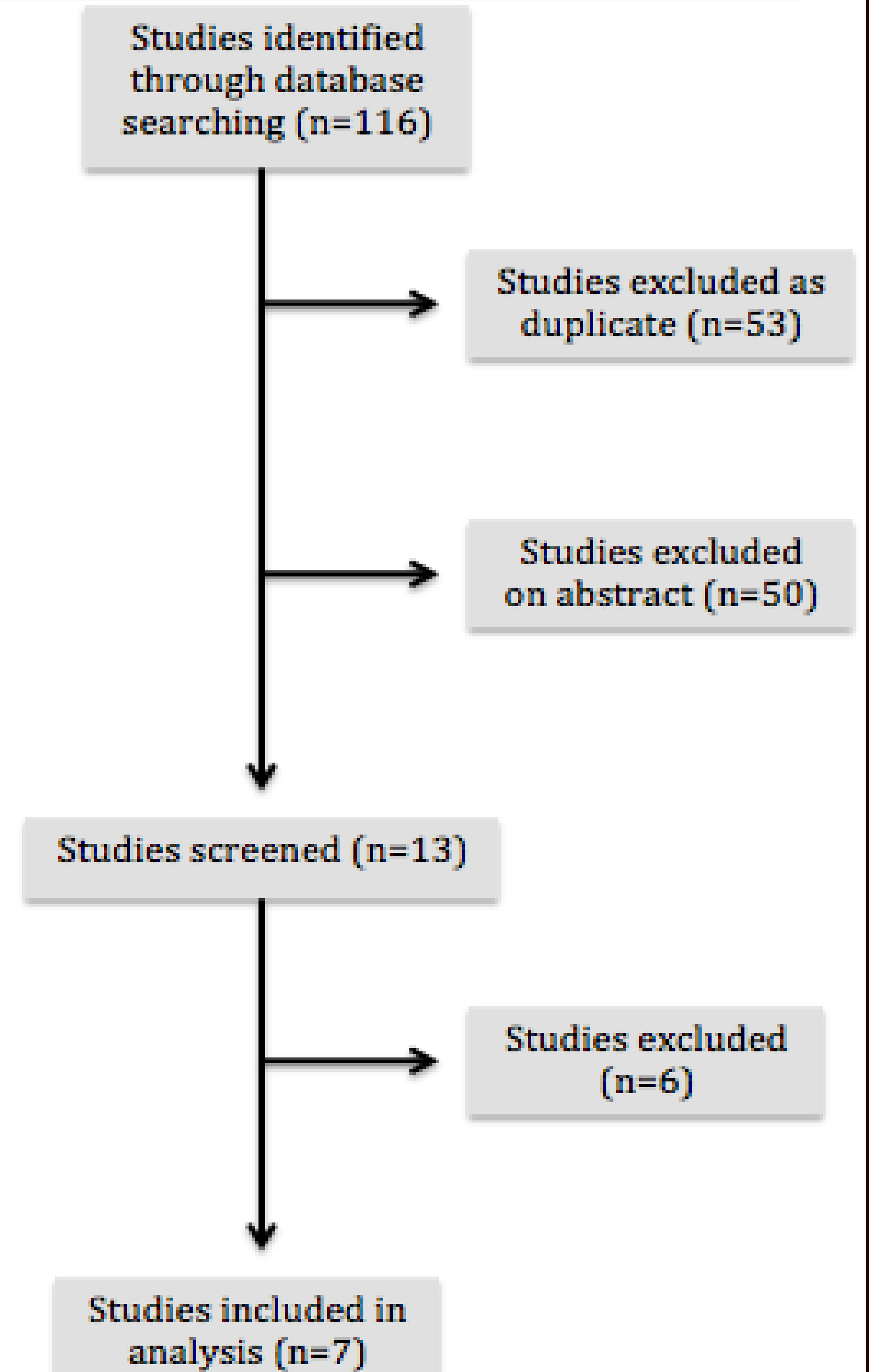
Abstract

Irreversible electroporation (IRE) uses multiple needles and a series of electrical pulses to create pores in cell membranes and cause cell apoptosis. One of the demands of IRE is the precise needle spacing required. Intraoperative 2D ultrasound (iUS) is currently used to measure inter-needle distances but requires significant expertise. This study evaluates the potential of 3D image guidance for placing IRE needles and calculating needle spacing.

A prospective clinical evaluation of a 3D needle localization system (Explorer™) was evaluated from April 2012 through June 2013 in consecutive patients who had IRE for unresectable pancreatic adenocarcinoma. 3D reconstructions of patients' anatomy were generated from preoperative CT images, which were aligned to the intra-operative space.

Thirty consecutive patients with locally advanced pancreatic cancer were treated with IRE. The needle localization system added an average of 6.5 minutes to each procedure. The 3D needle localization system increased surgeon confidence and reduced needle placement time.

IRE treatment efficacy is highly dependent on accurate needle spacing. The needle localization system evaluated in this study aims to mitigate these issues by providing the surgeon with additional visualization and data in 3D. The Explorer™ system provides valuable guidance information and inter-needle distance calculations.

Hypothesis

- The introduction of 3 dimensional navigation in IRE leads to increased confidence of the surgeon intraoperatively for proper identification of structures, appropriate needle placement and adequate ablation of target tissue.
- The aim of this study was to evaluate the use and feasibility of one of the commercially available image-guided surgery units intraoperatively and to assess if it provided clinically valuable information in the guidance of precise placement of IRE ablation needles

Methods

A literature review was completed after electronic searches were performed using PubMed and EMBASE electronic databases. The search was restricted to studies in English using a human model. The keywords used to search the database were navigation, pancreas/pancreatic, intra-operative and augmented reality. The references used in the studies that were identified were also reviewed.

To be included, studies had to be specifically about navigation surgery techniques involving the pancreas. Additionally, studies had to be from within the past seven years, in English and contain data about patients involved in the study. Duplicate articles were excluded. Figure 1 outlines the process used to select articles for the literature review.

The full text articles that met criteria were reviewed, with a focus on the type of navigation system used and how that was used intra-operatively, the outcomes noted in each study and the limitations and conclusions found in each study. These points of interest were compiled in a table for simple and quick comparison between articles.

A quality assessment of each article was performed using the Newcastle-Ottawa scale. A score from 0-9 is given to the articles based on the selection, comparability and outcome of group(s) involved in the study. A higher score on the Newcastle-Ottawa scale indicates a higher quality study.

Figure 1 (right): Flow chart illustrating how articles were found and identified as either appropriate for a literature review or eliminated from review.

Studies identified through database searching (n=116)
Studies excluded as duplicate (n=53)
Studies excluded on abstract (n=50)
Studies screened (n=13)
Studies excluded (n=6)
Studies included in analysis (n=7)

Results

Table 1: Information found during literature review organized

| Author and year	Type of navigation	Pre-op images used intra op	Organ	Primary outcomes	Secondary outcomes	Limitations	Conclusion	N-O scale
Okamoto et al. 2015	Augmented reality (AR) based navigation system with image overlay display	CT images used to construct a 3D model which was superimposed on the surgical field	Pancreas	No significant difference in operating time or intraoperative blood loss compared to conventional procedure	The position of each organ in the image created on the surgical field was nearly identical to the actual position of the organ	Registration accuracy, portability and cost	-AR based navigation contributed to accurate and effective pancreatectomy -This technology can improve surgical quality, training and education	6
Okamoto et al. 2015	Augmented reality (AR) based navigation system with image overlay display	Multi-detector CT, reconstructed in 3D using imaging software which are then viewed on a monitor by the surgeon intra-op	Pancreas	Organ identification and overlay precise to 6.8 mm	The usage of AR based navigation in GI surgery is a topic that needs further testing.	Organ deformity, evaluation of utility, portability, cost, time consumption	-Can be used as an effective teaching tool. -Allows for quick identification of structures	6
Onda et al. 2014	Augmented reality (AR) based navigation system with image overlay display	Multi-detector CT, reconstructed in 3D using software suite Analyze and displayed on a 3D monitor intra-op	Pancreas	No significant difference in operating time or intraoperative blood loss between group A who underwent identification of IPDA using AR, group B who underwent early ligation of IPDA without AR, group C who underwent conventional PD	No complications secondary to the navigation system were identified.	-Limited views of the images -Lack of tactile images	-Provides precise anatomical information -Allows for rapid identification of structures by the surgeon.	8
Onda et al. 2013	Augmented reality based navigation system using a short rigid scope and stereo-scope	Multi-detector CT reconstructed to overlay images in operative field after paired-point registration	Pancreas	No significant difference in operating time or intraoperative blood loss between cases where short rigid scope is used vs stereo-scope	No complications secondary to the navigation system were identified.	Organ shift and deformation.	-Short rigid scope and stereo-scope suitable for abdominal surgery. -System may improve safety, accuracy and efficiency of operations	8
Marzano et al. 2013	Augmented reality (AR) based navigation system with image overlay display	CT; 3D model created using software VR-RENDER, IRCAD; superimposed on operative field using Exoscope	Pancreas	Operative time was 360 minutes. AR display and fine registration was performed within 6 minutes	No complications secondary to the navigation system were identified.	-Fusion of virtual model and intra-op images. -Update rate of the 3D virtual model	AR can enhance the ability to safely perform resection during PD.	8
Volonte et al. 2011	Augmented reality (AR) based navigation system with image overlay display	3D reconstructions created from CT using OsiriX software and projected onto the operative field	Gall bladder; Pancreas	AR improved identification of target structures	AR can reduce intraoperative risks and complications	Organ shift	-Can be used as an effective teaching tool. -Can make surgical interventions easier, faster and possibly safer.	6
Sugimoto et al. 2010	Augmented reality (AR) based navigation system with image overlay display	3D reconstructions created from CT using OsiriX software and projected onto the operative field	Gall bladder Colon Stomach Pancreas	Fewer intraoperative injuries and less bleeding encountered with use of image overlay.	No complications secondary to the navigation system were identified.	Cost, system operation difficulty, time for registration	-Using markers on the body surface reduces logistical efforts -Image overlay is useful in highlighting structures	8
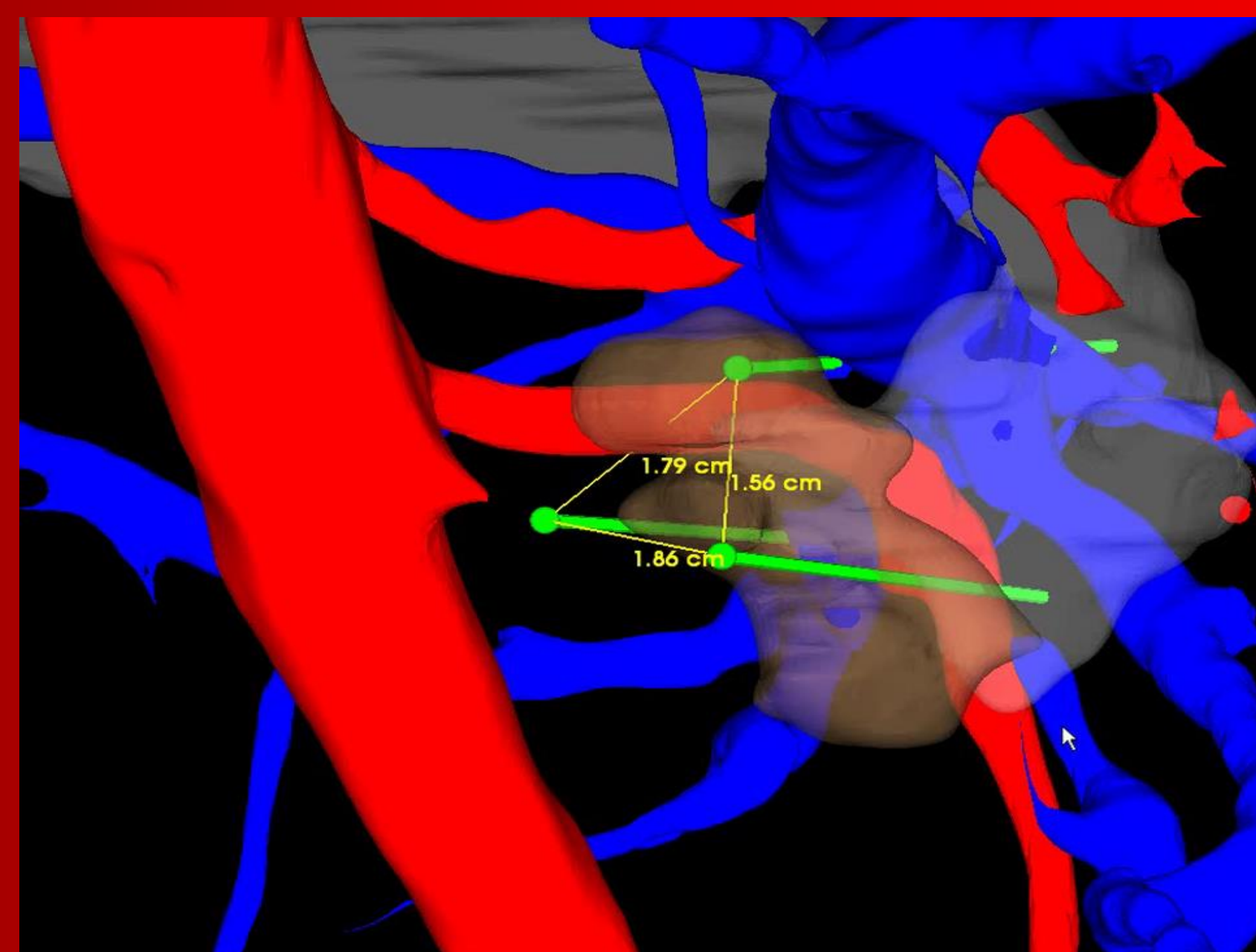
Figure 2 (above): Images comparing the 3 dimensional image guided system versus the traditionally used intraoperative ultrasound during IRE.

Table 2 (below): Questionnaire given to surgeons after using the 3 dimensional imaging system during IRE.

Category	Average	Min	Max
Needle localization error (relative to iUS baseline, mm)	3.4	0.3	11.7
Questionnaire	Yes	No	
Did the system increase your confidence in the placement of each needle?	8	6	
Were the tomographic views (axial, coronal, sagittal CT) valuable?	13	1	
Were the 3D models valuable?	11	3	
Did the localization system reduce time required to place each needle?	8	6	
Were there any ease of use obstacles?	10	4	

Conclusion

- The needle localization system increased surgeon confidence in over 50% of procedures and and was felt to reduced needle-placement time in 60% of procedures when compared to procedures w/o 3D reconstruction.
- IRE is technically demanding nd the efficacy of treatment is largely dependent on proper needle placement.
- Intraoperative navigation system allows for additional measurements and visualization while also potentially decreasing operative time.

Acknowledgements

Small Molecule Inhibition of Choline Kinase-α Decreases Proliferation Of Non-Small Cell Lung Cancer

Andrew Bratton, Jason Chesney, Sucheta Telang

Molecular Targets Program, James Graham Brown Cancer Center, University of Louisville School of Medicine

Introduction

Non-small cell lung cancers (NSCLC) exhibit significantly elevated levels of phosphocholine relative to adjacent normal lung tissue. The overexpression of phosphocholine in malignant cells is largely due to the activity of the Ras and PI3K signaling cascades, which stimulate the production of the enzyme choline kinase-α (ChK-α) via the Rho GTPases. ChK-α executes the first committed step in the Kennedy pathway that allows for the biosynthesis of phosphatidylcholine, which serves as the major phospholipid constituent of cellular membranes and a substrate for the production of phosphatidic acid for subsequent growth factor signaling. In previous studies, we found that selective silencing of ChK expression abrogated the expression of phosphocholine which, in turn, decreased phosphatidylcholine, phosphatidic acid and signaling through the MAPK and PI3K/AKT pathways and led to a marked decrease in anchorage-independent survival of cancer cells in soft agar and in athymic mice. We hypothesized that targeting ChK-α with a small molecule inhibitor (termed CK1) may prove to be an effective antineoplastic strategy.
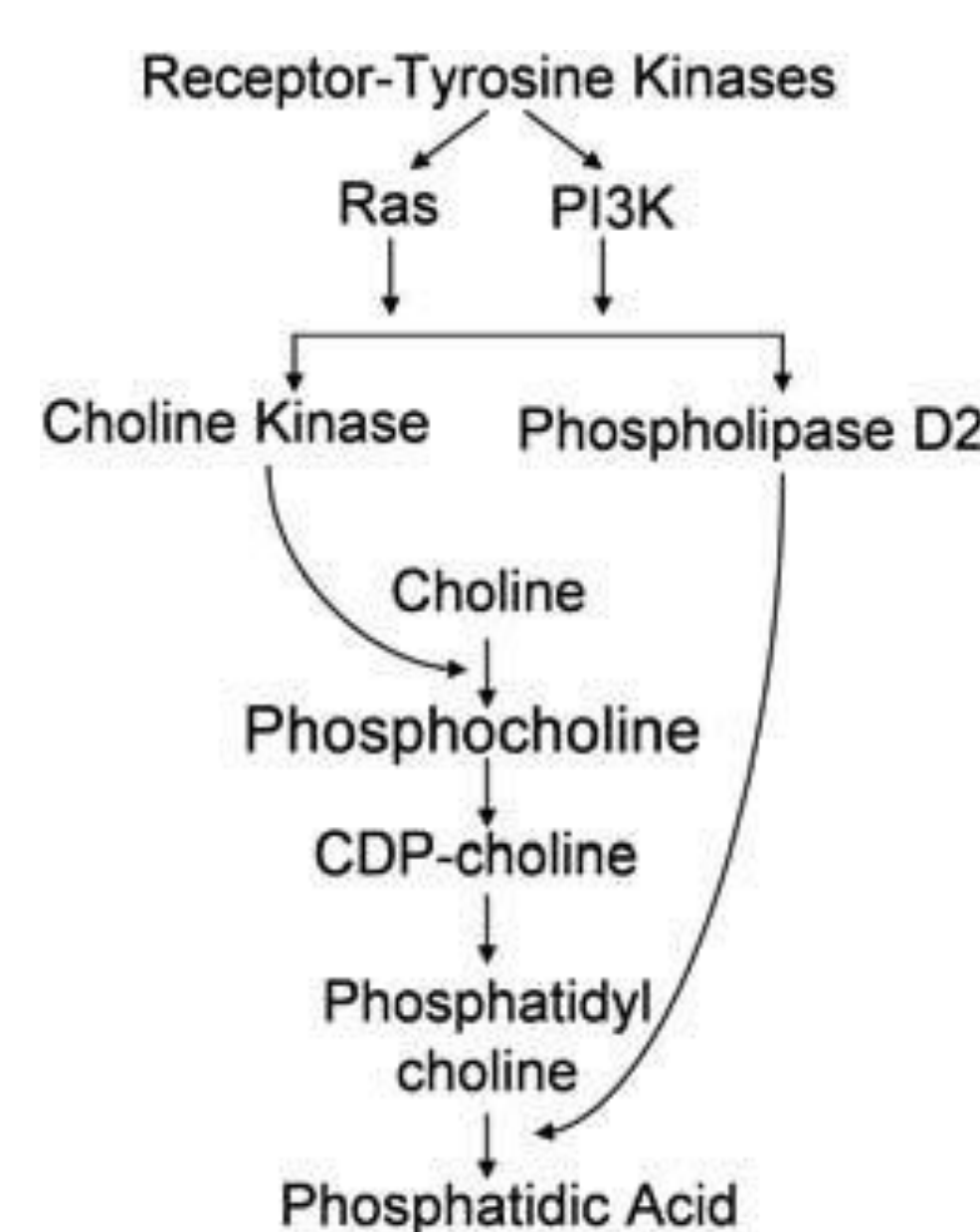
Objectives

- Assess the anti-proliferative effects of the small molecule ChK-α antagonist, CK1, on NSCLC cell lines.

- Determine the effect of CK1 on apoptosis.

- Examine the relationship between ChK-α protein expression and response to CK1 exposure .
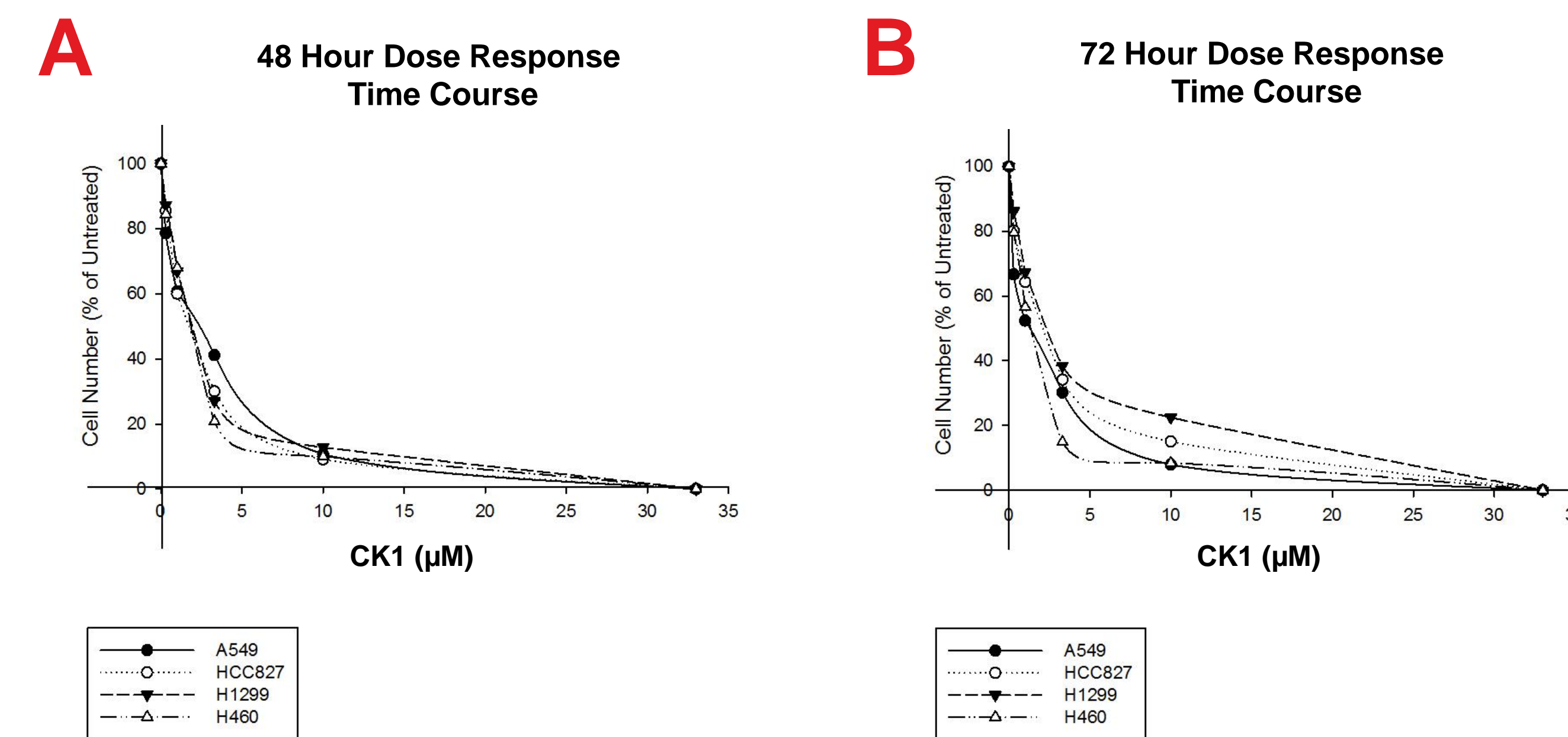
Results

Figure 1. Changes in cell proliferation of NSCLC lines (A549, HCC827, H1299, and H460) at 48 hours in response to increasing concentrations of CK1 (0-33 µM) (A) was determined by staining with Trypan blue then manually counting. The effects at 72 hours (B) were also examined. All the cell lines had an IC50 <3.3 µM, and H460 cells were the most sensitive of all four cell lines to the anti-proliferative effects of CK1.
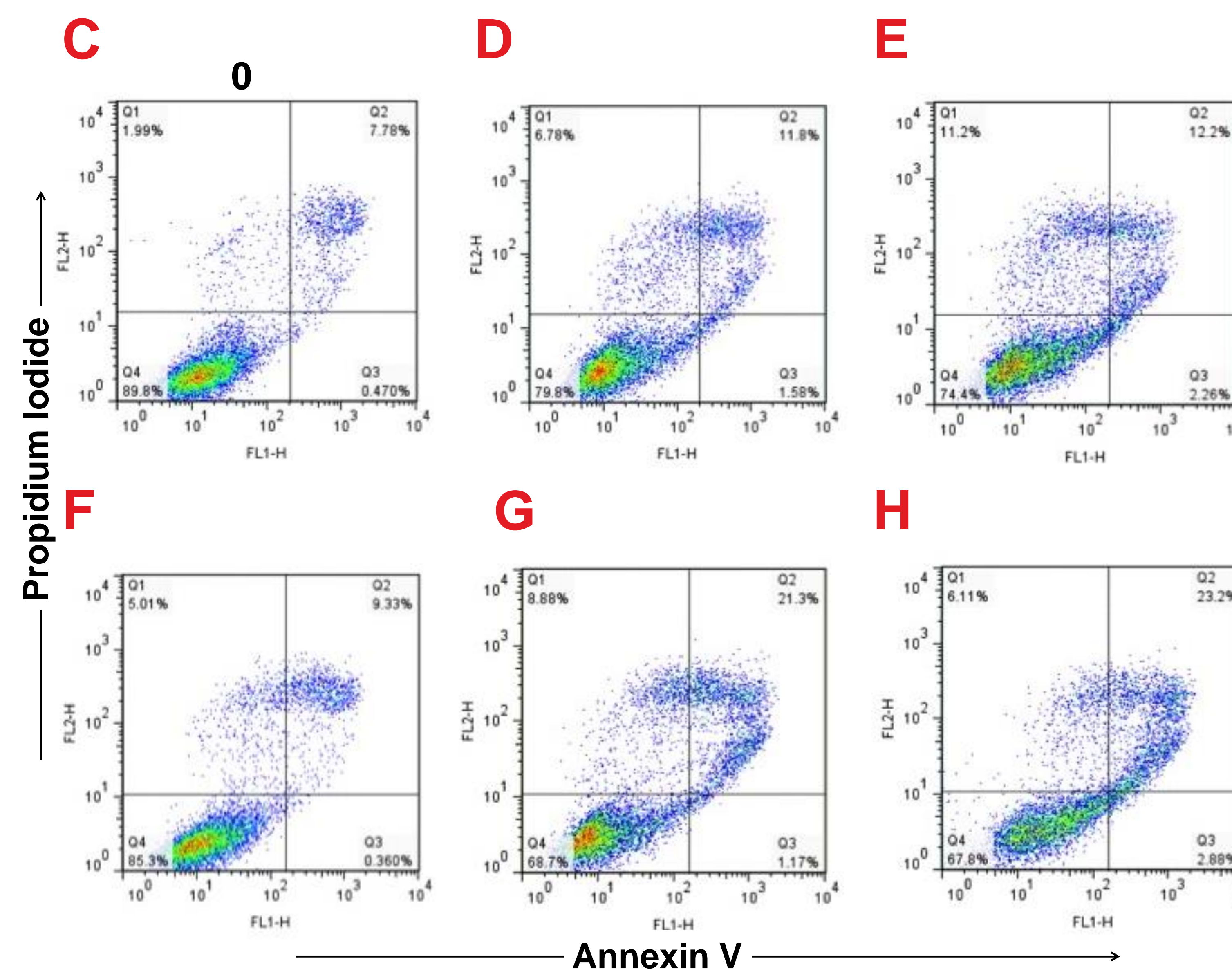

Figure 2. H460 cells were exposed to increasing concentrations of CK1 and apoptosis and necrosis examined by flow cytometry following annexin V/propidium iodide staining. At 48 hours, H460 cells showed an increase in apoptosis (FL1-H) and necrosis (FL2-H) with an increase in CK1 from 0 (C) to 3.3 (D) to 10 µM (E). At 72 hours (F-H), we noted a more pronounced increase in apoptosis and necrosis.
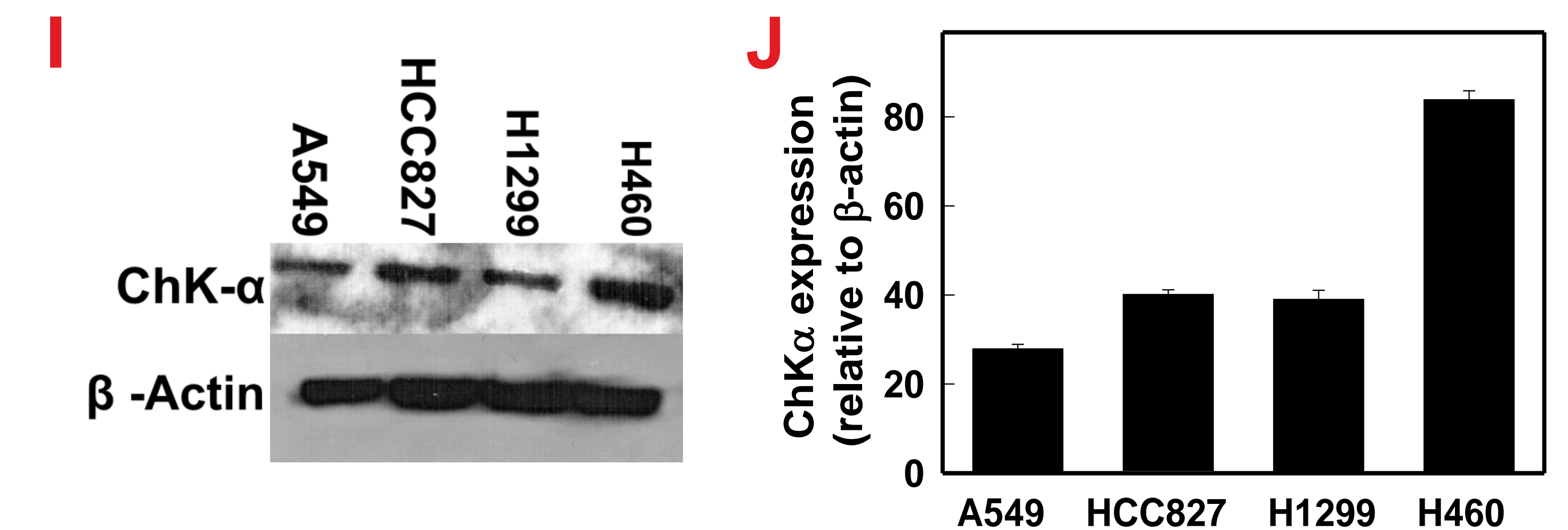

Figure 3. ChK-α protein expression in four NSCLC cell lines (I) was determined by Western blot analysis. Higher expression of ChK-α protein was noted in H460 and HCC827 cells than in A549 and H1299. β-Actin was used as the loading control. (J) Densitometry conducted (with ImageJ) and normalized to β-Actin. High levels of ChK-α expression corresponded with greater sensitivity to CK1 treatment.

Conclusions

- Treatment with CK1 significantly inhibited the growth of four NSCLC cell lines in a dose and time-dependent manner (Figure 1).

- H460 cells demonstrated a dose dependent increase in apoptosis and necrosis after 48 hours of exposure to CK1 and a more pronouced increase after 72 hours (Figure 2).

- Cell lines with greater ChK-α protein expression may be more responsive to CK1 treatment (Figure 3).

Acknowledgements

Radioprotective Effects of Ferritin

Phillip Burkhardt; Lilibeth Lanceta; Patricia Soucy, Ph.D.; Chi Li, Ph.D.; John Eaton, Ph.D.
Molecular Targets Program, James Graham Brown Cancer Center, University of Louisville

Abstract

The National Aeronautics and Space Administration (NASA) has its sights set on a manned Mars mission, a mission requiring up to three years of space travel. Astronauts will be exposed to substantial radiation. Prolonged exposure to linear energy transfer (LET) radiation, emitted from our sun and other stars, damages DNA and kills cells partly through iron-dependent reactions. In a recent study, Haro et al. (PLOS ONE 7:11/e48841, 2012) selected for human myeloid leukemia HL60 cells resistant to low energy LET and found >12-fold reduction in expression of Iron Regulatory Protein-1 (IRP-1), an important negative regulator of ferritin synthesis. As an intracellular iron storage protein up-regulated by IRP-1 decrease, ferritin is a likely mediator of radioresistance. Increased cellular ferritin may lead to radioresistance through decreasing radiation-induced, iron-mediated, Fenton chemistry and DNA damage from low energy LET radiation. Given that exposure of astronauts to radiation in space during a Mars expedition is likely to lead to a 10-15% increase in cancer risk, pharmacologic strategies to increase ferritin expression might provide a measure of protection. Our research indicates that treatment with the compound 1,2-dithiole-3-thione (D3T), known to induce ferritin, leads to radioprotection of cells. This treatment has promise as a radio-protectant. A related compound, Oltipraz, is currently an FDA approved medication.
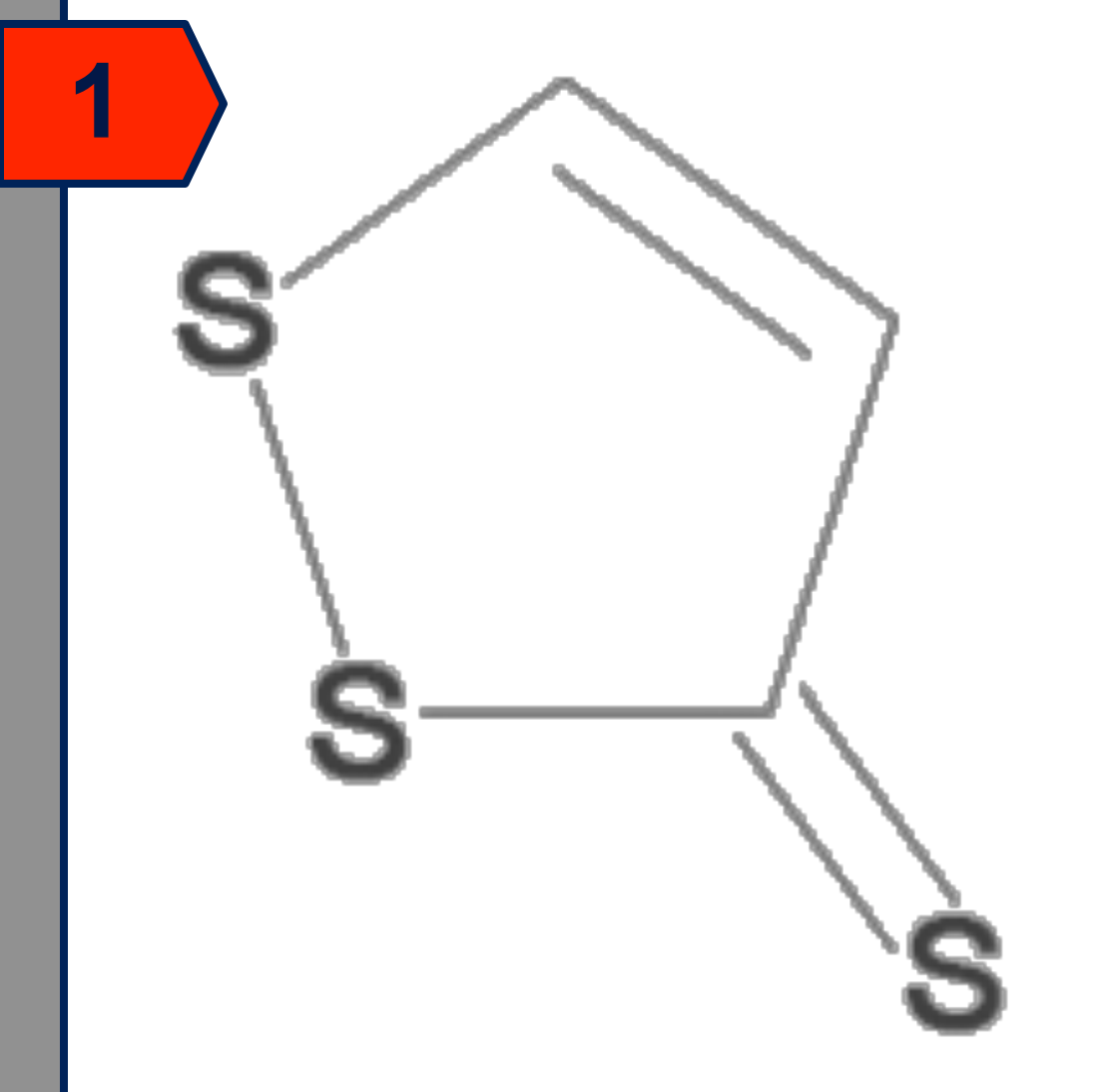
1

Figure 1

1,2-dithiole-3-thione (D3T) Compound Structure

Results

2

D3T Induces Ferritin Synthesis

Cells   DMSO   D3T

FTH1

Actin

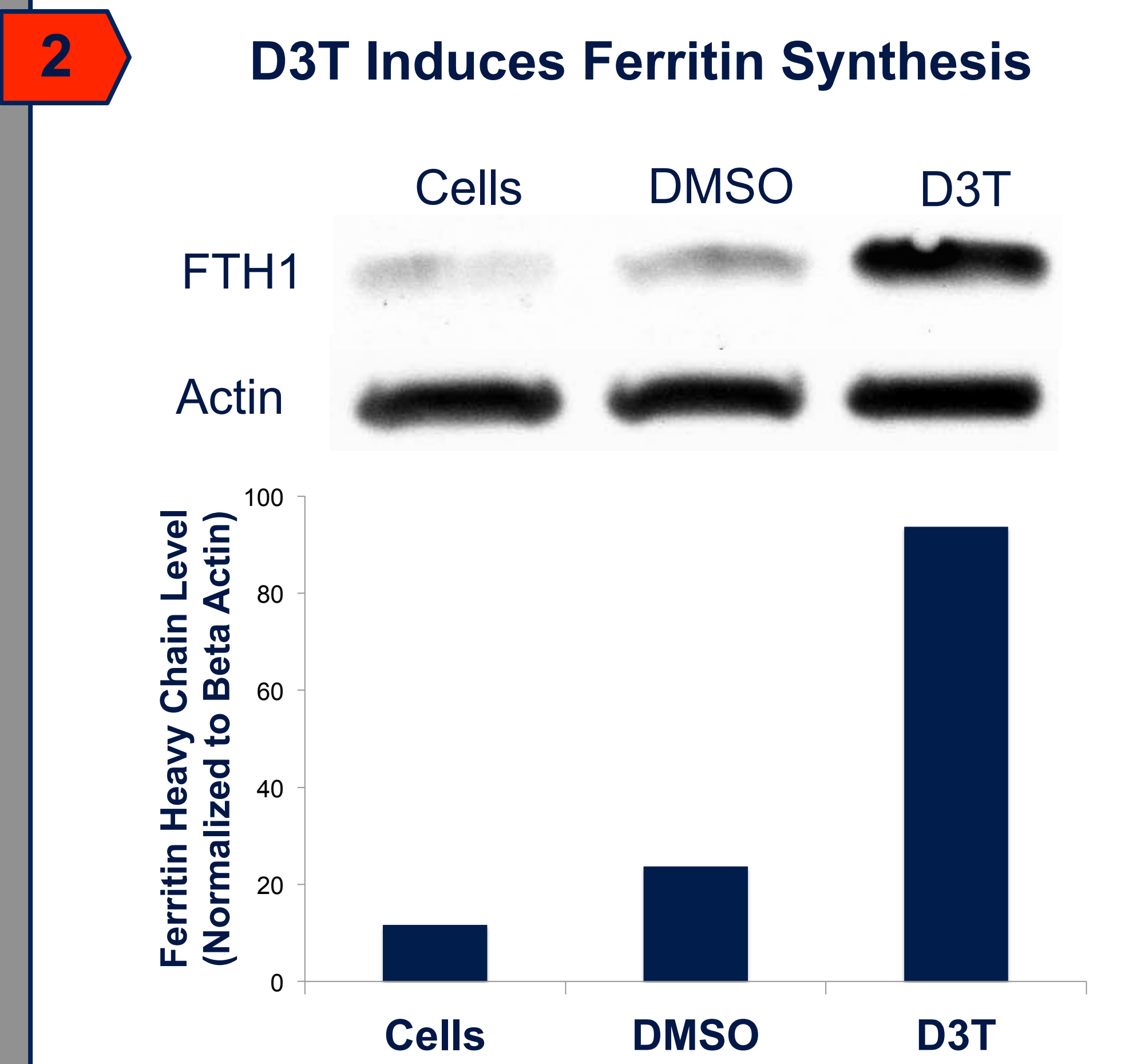Ferritin Heavy Chain Level (Normalized to Beta Actin)

Figure 2

D3T (1,2-dithiole-3-thione) Induces Heavy Chain Ferritin Synthesis: NIH 3T3 cells were plated in a 6-well plate (7.0x10^5 cells/well) then treated with 70µm D3T for 24 hours. Cells where harvested, measured with BCA, 20µg of protein was loaded in 4-20% TGX gradient gel. The blot was probed with rabbit anti-mouse heavy chain ferritin antibody (1:1000) overnight in 4°C. Beta actin used as loading control
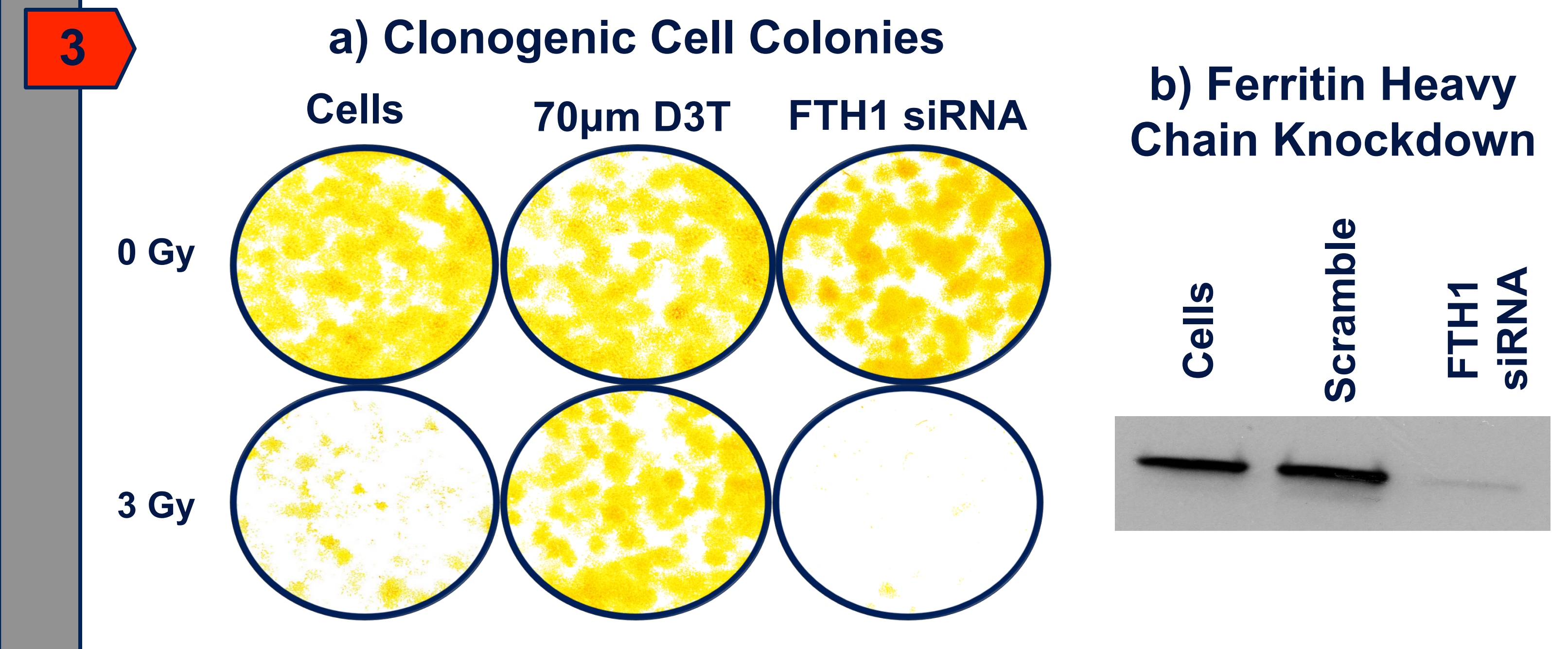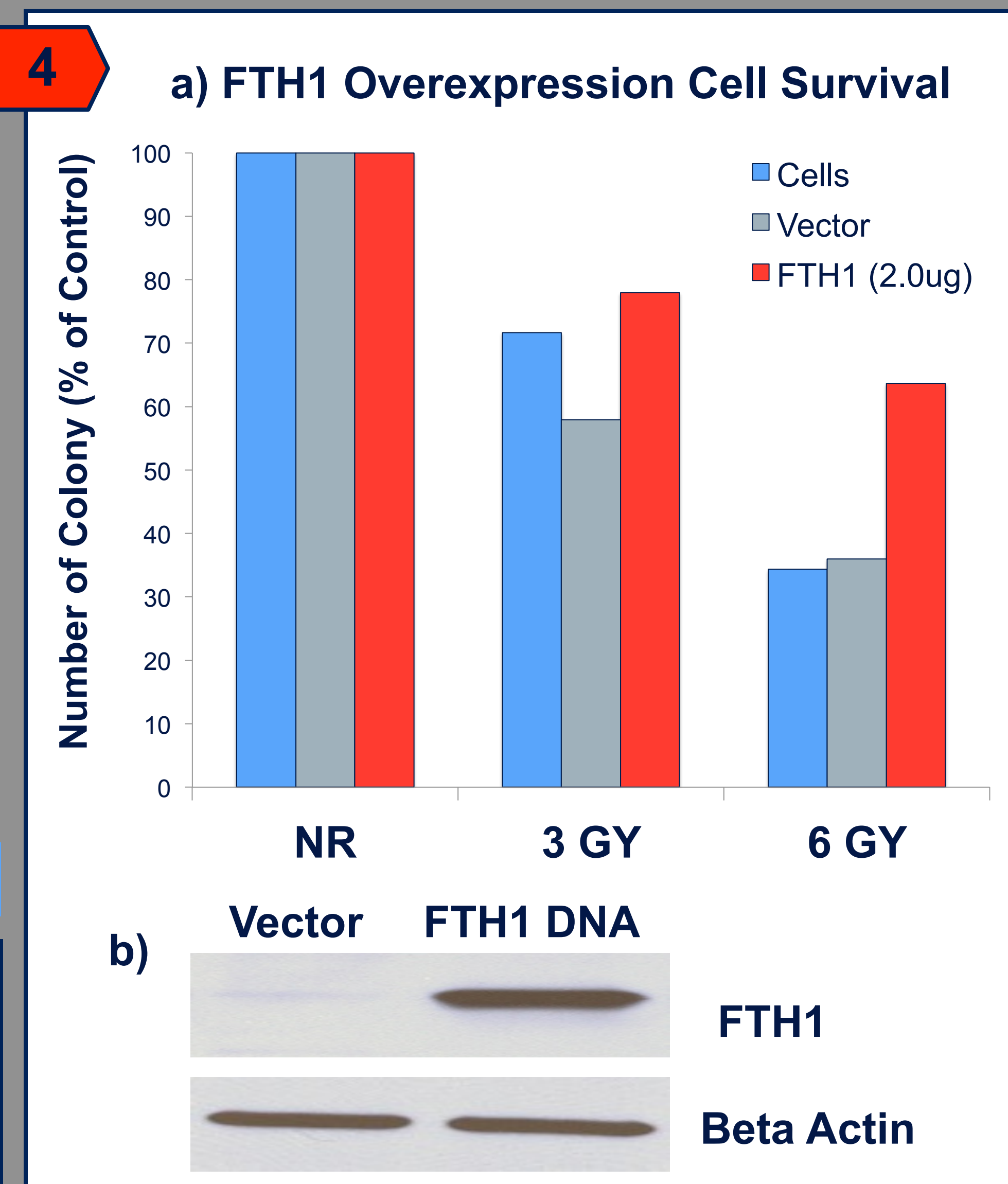
3

a) Clonogenic Cell Colonies

Cells   70µm D3T   FTH1 siRNA

0 Gy

3 Gy

b) Ferritin Heavy Chain Knockdown

Cells   Scramble   FTH1 siRNA

Figure 3

a) Clonogenic Cell Colonies: NIH 3T3 cells were plated in T25 flask (6.0x10^4 cells/flask). Cells were treated with either 70µm D3T or 10nm FTH1 siRNA for 24 hours. Cells then received irradiation of either 0Gy or 3Gy. The next day cells were plated in 6-well plates (500 cells/well) for clonogenic survival assay, grown for 10 days, then stained with 0.5% crystal violet.

b) Ferritin Heavy Chain Knockdown: NIH 3T3 cells, transfected with 10nm FTH1 siRNA for 24 hours. Measured with BCA, 20µg of protein in 4-20% TGX gradient gel. Probed with rabbit anti-mouse heavy chain ferritin antibody (1:1000) overnight, 4°C.
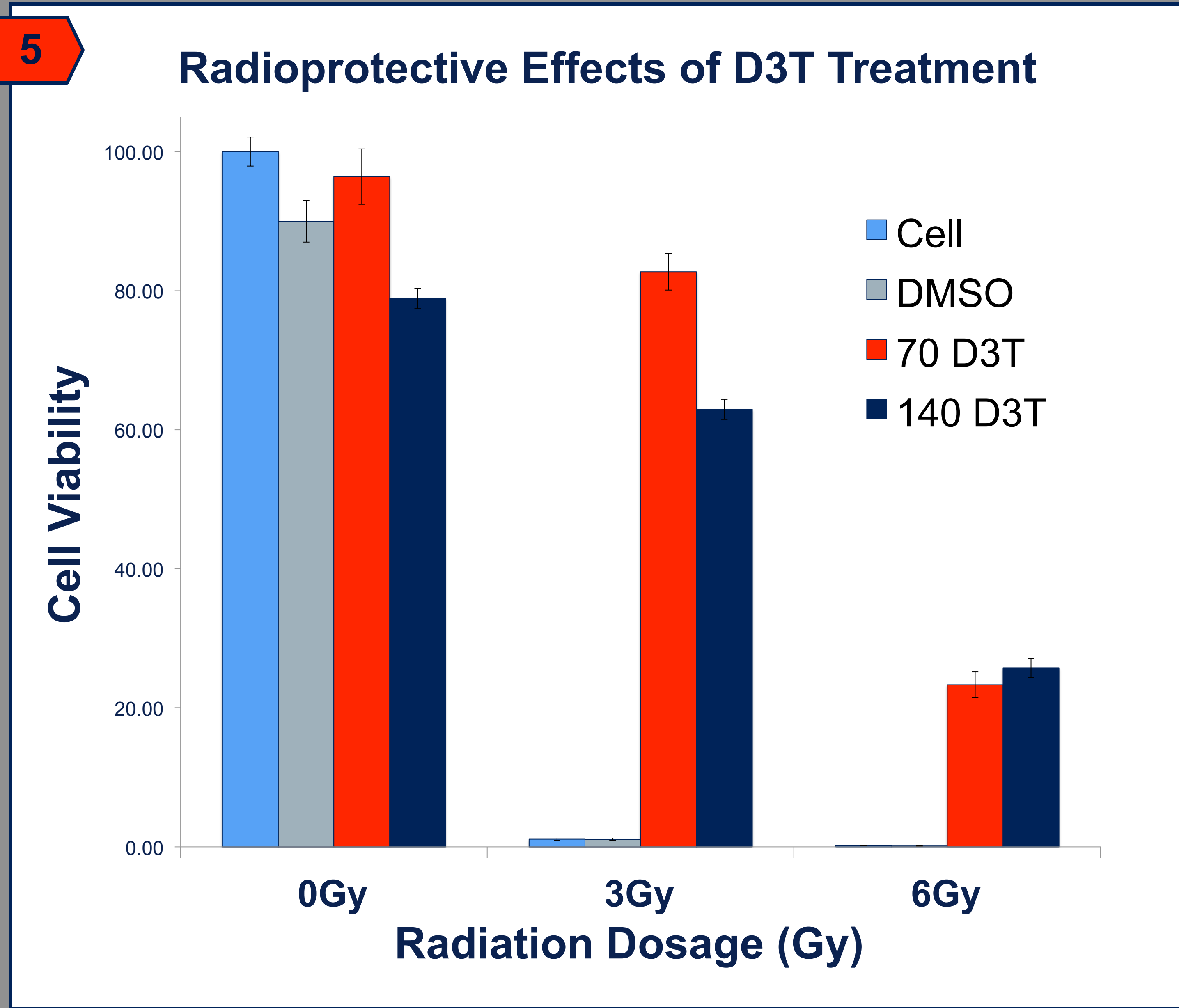
4

a) FTH1 Overexpression Cell Survival

Number of Colony (% of Control)

Cells
Vector
FTH1 (2.0ug)

NR   3 GY   6 GY

b)

Vector   FTH1 DNA

FTH1

Beta Actin

Figure 4

a) FTH1 Overexpression Cell Survival: NIH 3T3 cells were plated in T25 flasks (1.5x10^5 cells/flask). Either treated with 2.0µg FTH1 plasmid DNA or vector for 24hr, then irradiated at 0, 3, or 6 Gy. 24 hours later cells were replated in 6-wll plates (500 cells/well). After 10 days, stained with 0.5% crystal violet for clonogenic assay.

b) Ferritin Heavy Chain Overexpression: 20µg of vector and plasmid treated NIF 3T3 cell protein was ran in a 4-20% TGX gel, beta actin as loading control

5

Radioprotective Effects of D3T Treatment

Cell Viability

Cell
DMSO
70 D3T
140 D3T

0Gy   3Gy   6Gy

Radiation Dosage (Gy)

Figure 5

Radioprotective Effects of D3T Treatment: NIH 3T3 cells were plated in T25 flask (7.0x10^4 cells/flask). Cells were treated with either 70µm or 140µm D3T for 24 hours. Cells then received irradiation of either 0, 3, or 6Gy. The next day cells were plated in 6-well plates (500 cells/well) for clonogenic survival assay, grown for 10 days, then stained with 0.5% crystal violet.

Conclusions

1. Treatment with D3T can increase cellular resistance to radiation.

2. Increased cellular ferritin is a probable factor of protection given that D3T increases ferritin production and the knockdown of the ferritin heavy chain (FTH1) mRNA leads to greater radio sensitivity.

Further Research

1. Treat cells with D3T and FTH1-knockdown simultaneously to solidify ferritin's role in radioprotection.

2. Exploring ferritin induction through Iron Regulatory Protein (IRP-1) knockdown.

3. Furthering testing of D3T-mediated radioprotection in vivo by administration of D3T to mice.

Acknowledgements

The Interplay between Aging and Lung Inflammation / Remodeling in Lung Cancer Progression

Aneesha Carter[1], John C. Greenwell[2], E Torres-González[3], Glenn Vicary[2], Jeff Rizenthaler[3], Jesse Roman[2,3,4]

[1]NCI Cancer Research Program, [2]Department of Pharmacology and Toxicology, [3]Department of Medicine, Division of Pulmonary, Critical Care and Sleep Disorders Medicine, University of Louisville School of Medicine and [4]Veterans Affairs Medical Center, Louisville, KY.

ABSTRACT

Rationale: Lung cancer is the leading cause of cancer-related deaths in the world. Although new information about lung cancer is developing at an increasing pace, its 5-year survival rate remains at a bleak 15%. Due to its rapid progression and low survival rate, lung cancer continues to be the center of many investigative efforts hoping to uncover specific targets for intervention. **Hypothesis:** Most lung cancers develop in elderly people with chronic lung disease characterized by chronic inflammation and tissue remodeling. Thus, we hypothesize that aging and lung inflammation/remodeling act in concert to promote lung cancer progression. **Methods:** To test this hypothesis, we utilized a xenograft model of experimental lung cancer in C57BL/6 male mice. These mice were treated with *bleomycin*, which is a well-known lung injury model characterized by an early inflammatory phase that peaks 7 days after the initial intratracheal injection of bleomycin. The inflammatory phase is followed by a fibrotic phase that peaks 14 days after the initial bleomycin injection. To evaluate the effects of aging, young (3.7 months of age) and aging (9.5 months of age) mice were injected with Lewis Lung Carcinoma (LLC) cells (1×10^6, S.C) 14 days after initial bleomycin instillation. Additionally, *in vitro* cell culture studies were conducted utilizing primary lung fibroblast-conditioned media and analysis of cell proliferation, migration, and apoptosis on the LLC cells. **Results:** *In vitro* studies indicated that fibroblast-conditioned media promotes LLC cell proliferation and protects against Cisplatin induced cell death. This suggests that products derived from stromal cells influence lung cancer. Using the xenograft model, we found that untreated aging mice developed more lung metastases than young mice. We then turned our attention to the effects of bleomycin and found that, as expected, bleomycin induced weight loss and lung inflammation/remodeling in both young and aging mice. When tumors were implanted in bleomycin-treated animals, the size of the subcutaneous tumors were similar at the time of euthanasia (p = 0.2). As before, aging animals treated with bleomycin developed more metastases when compared to young mice. Importantly, bleomycin treatment further enhanced the number of metastases in the aging mice when compared to untreated aging animals (p=0.0002). **Conclusion:** Our studies suggest that age-dependent host factors influence lung cancer progression, and that lung fibroblasts might be responsible for some of these events. Importantly, based on studies in the bleomycin model, we conclude that lung inflammation and tissue remodeling enhance pulmonary metastasis in the aging lung, but not in the young lung, thereby indicating an interplay between lung aging and inflammation/remodeling in experimental tumor progression.

BACKGROUND

Lung cancer is the leading cause of cancer-related deaths for both men and women and is estimated to kill 160,000 Americans in 2015.[1] There are numerous risk factors that have been linked to lung cancer such as tobacco smoke, exposure to environmental toxins, genetic conditions, and chronic lung disease including pulmonary fibrosis. Contributing factors may promote oxidative stress and aberrant tissue remodeling, possibly increasing the susceptibility of the lung to cancer metastasis.

Immune cells and their products during inflammation have been implicated in cancer progression. Similarly, fibroblasts are known to produce extracellular matrices that can influence cancer cell behavior. These extracellular matrix proteins, such as fibronectin and collagen, provide structural support to cells, affect tissue stiffness, and may serve as mitogens for tumor cells. In disease states characterized by overexpression of extracellular matrices (e.g., lung fibrosis), these events might be amplified, thereby promoting tumor progression via metastasis. Aging, has also been implicated in cancer development and progression, and most lung cancers occur in the elderly, but the factors responsible for this effect remain incompletely elucidated.

Here, we use young and aging mice as well as the bleomycin model of lung injury in conjunction with a xenograft model of lung cancer to study the role of aging and inflammation/remodeling in lung cancer progression.

HYPOTHESIS
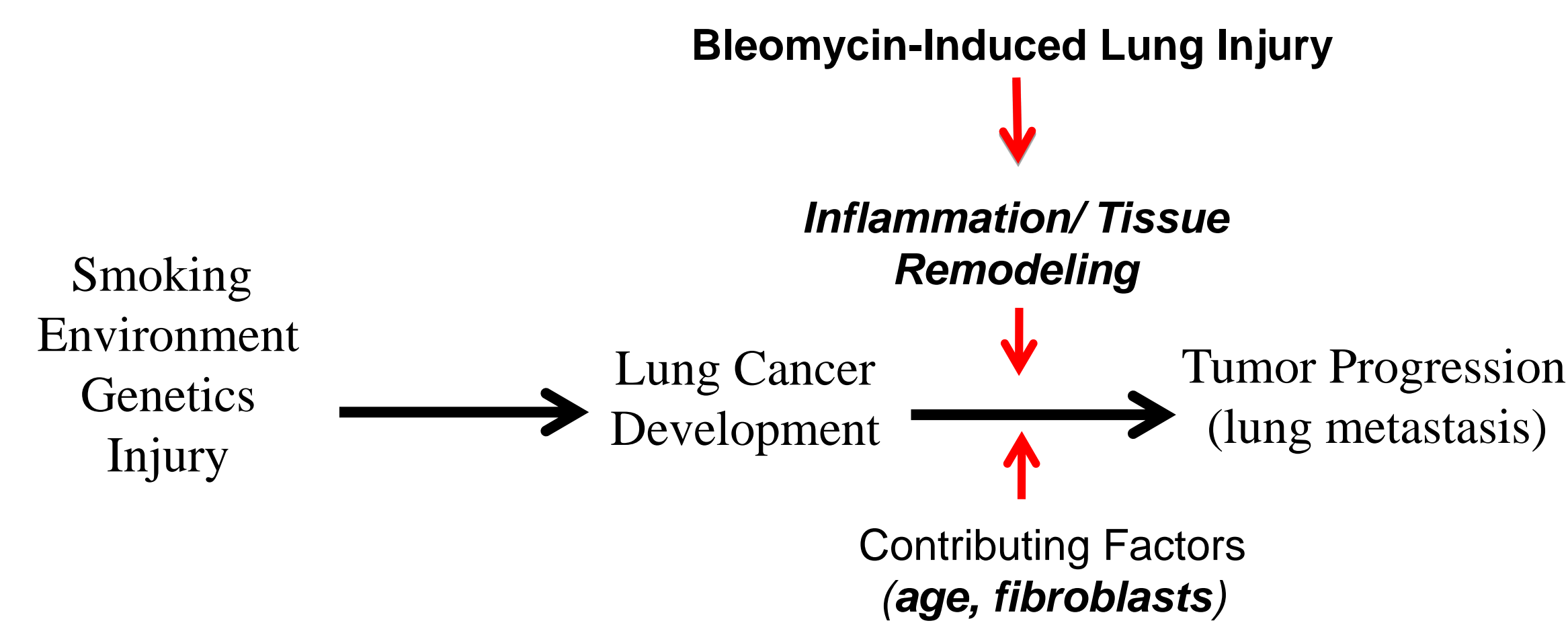
Aging and lung inflammation / tissue remodeling promote lung cancer progression

RESULTS

I. Cancer cell proliferation, migration was affected by fibroblast-conditioned media
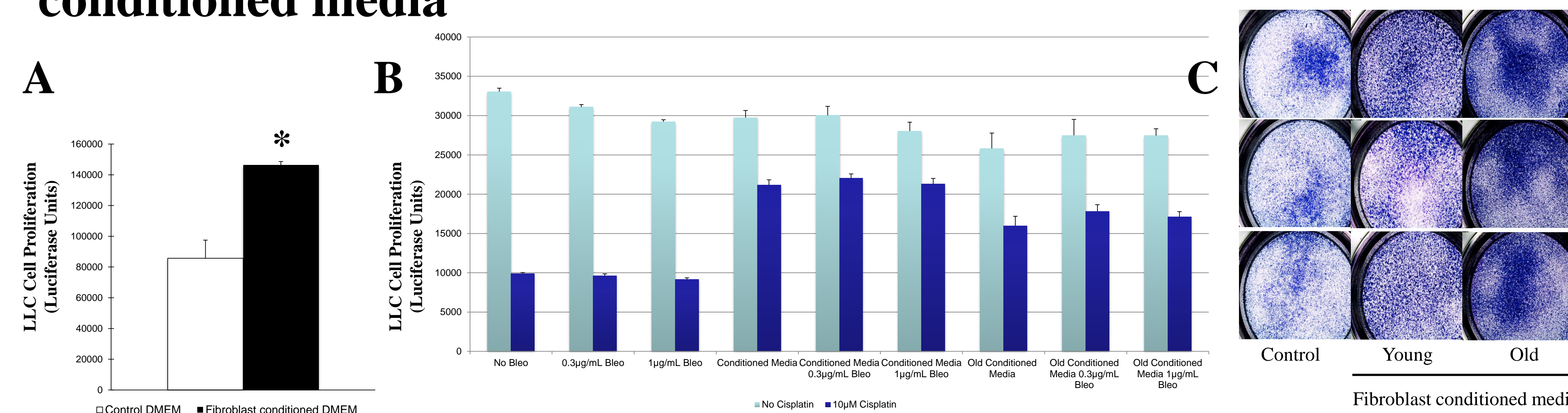

Figure 1: **(A)** LLC cells (500/well) exposed to control DMEM or fibroblast conditioned media (primary mouse lung fibroblasts) for 48 hours. * p<0.05, N=5 for each group. **(B)** LLC cells (4000/well) exposed to control DMEM or conditioned media from fibroblasts treated with bleomycin were exposed to Cisplatin. Viable cells were detected using Cell Titer-Glo Luminescent Cell Viability Assay (Promega). **(C)** LLC cell migration after exposure to control DMEM or fibroblast-conditioned media.

II. Bleomycin induced weight loss in mice (A), but did not affect tumor size at the site of implantation (B)
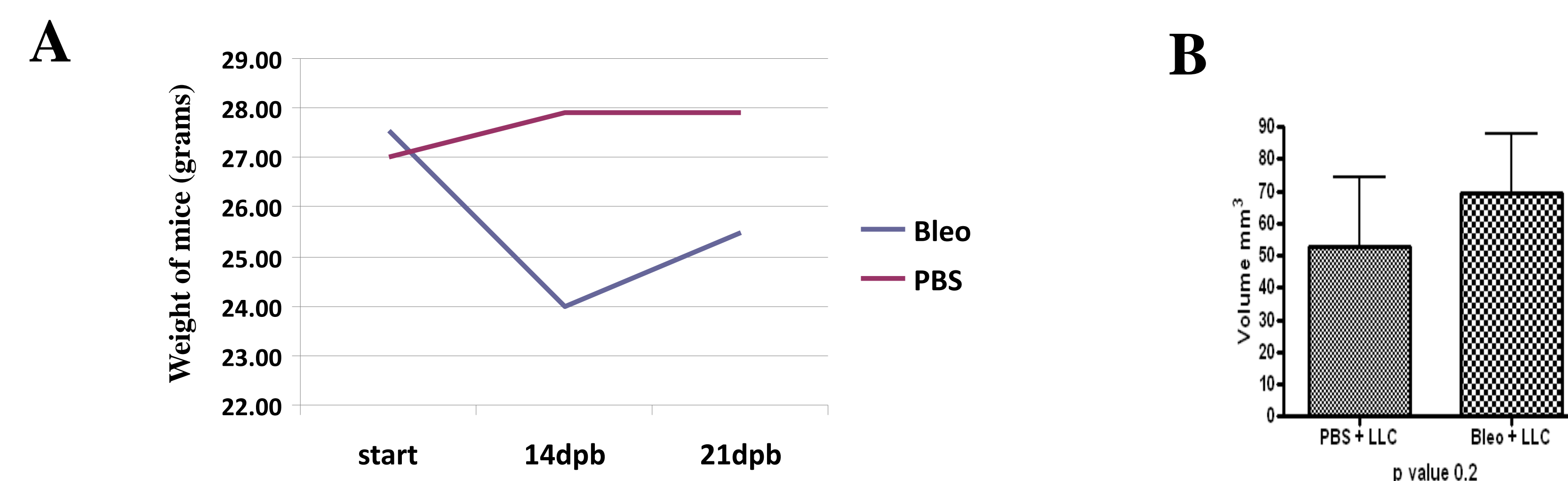

Figure 2: **(A)** The change in weight in mice treated with bleomycin+LLCs and PBS+LLCs mice was analyzed. In bleomycin+LLCs treated mice, the weight of the mice decreased significantly. The difference in weight loss in young and old PBS+LLCs and Bleomycin+LLCs treated mice was not statically relevant. **(B)** The size of the tumors at the site of implantation was evaluated. There were no differences in size of tumor in PBS vs. Bleo treated mice.

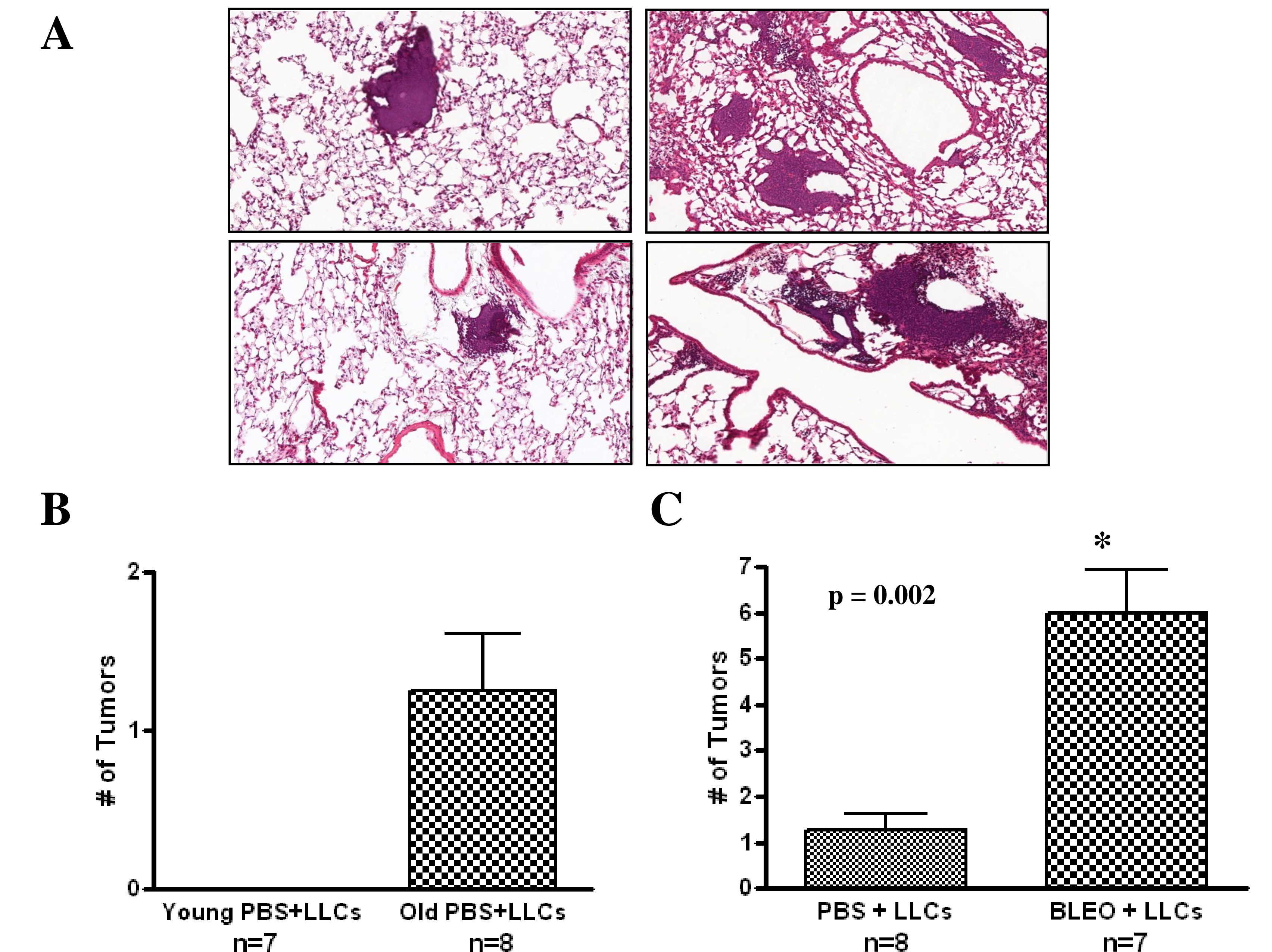### III. Lung metastasis increased in Bleomycin-treated old mice

Figure 3: Lung metastasis was analyzed in young vs. aging male mice treated with PBS versus bleomycin **(A)** Images depict PBS- and bleomycin (BLEO)-treated aged mice at 14x magnification. **(B)** Aging mice showed more lung metastases than young mice. **(C)** Bleomycin-treated aging mice showed more lung metastases than untreated aging mice. Lung Metastases 30 days post PBS or bleomycin treatment and 16 days post LLC injection.

Summary

- Fibroblast-derived products promote LLC cell proliferation, protects against exposure to Cisplatin.
- Aging mice show more lung metastases than young mice.
- Bleomycin further enhances the effects of aging with regards to metastases.

Conclusion

These studies suggest that age-dependent host factors influence lung cancer progression, and that lung fibroblasts might be responsible for some of these events. Importantly, lung inflammation and tissue remodeling may enhance pulmonary metastasis in the aging lung, but not in the young lung, thereby indicating an interplay between lung aging and inflammation/remodeling in experimental tumor progression.

Acknowledgments

Effect of Arylamine *N*-acetyltransferase 1 Knockout by CRISPR/Cas 9 on Doubling Time in MDA-MB-231, MCF-7, & ZR-75-1 Breast Cancer Cell Lines

Maggie Y. Chang, Marcus W. Stepp, Mark A. Doll, and David W. Hein

Department of Pharmacology & Toxicology and James Graham Brown Cancer Center

University of Louisville, Louisville, Kentucky

UNIVERSITY OF LOUISVILLE It's Happening Here.

Abstract

About 1 in 8 women will develop invasive breast cancer over the course of her lifetime according to BreastCancer.Org. Human arylamine *N*-acetyltransferase 1 (NAT1) is found in almost all tissues and is overexpressed in breast cancers. Previous studies have shown great variation in NAT1 activity among various breast cancer cell lines with MDA-MB-231 < MCF-7 <<< ZR-75-1. We hypothesize that human NAT1 has a role in cancer cell proliferation or progression and that knockout of arylamine *N*-acetyltransferase 1 (NAT1) will increase the doubling time of MDA-MB-231, MCF7 and ZR breast cancer cell lines. Human NAT1 activity was measured in parent MDA-MB-231, MCF-7, and ZR-75-1 breast cancer cell lines before (parent cell line) and after NAT1 knockout by CRISPR/Cas 9. PABA NAT1 activities in the parent breast cancer cell lines were in the order MDA-MB-231 < MCF-7 <<< ZR-75-1 but were below the limit of detection in each of the breast cancer cell lines following NAT1 knockout. Significant changes in doubling time in the MDA-MB-231 or MCF-7 knockout clones relative to the parent cell line were not observed. The ZR-75-1 NAT1 knockout cell line showed nearly a 2-fold increase in doubling time compared to the parent, but this did not reach statistical significant perhaps due to small sample size. Since the ZR-75-1 breast cancer cell line has the highest NAT1 activity compared to other cell lines, our results suggest the effect of NAT1 knockout on doubling time is more pronounced in breast cancer cells with high levels of NAT1 activity. Further investigations are needed to confirm this hypothesis. This work was partially supported by USPHS grant CA-134283 from the National Cancer Institute.

Hypothesis

We hypothesize that CRISPR/Cas9 knockout of arylamine *N*-acetyltransferase-1 (NAT1) will increase the doubling time in MDA-MB-231, MCF-7, and ZR-75-1 breast cancer cell lines.

Introduction

-5 year survival rate for breast cancer diagnosed at localized stage is 98.5% but at distant stage the 5-year survival is roughly 25% (1).

-Arylamine *N*-acetyltransferase 1 (NAT1) is a phase II xenobiotic metabolizing enzyme that plays an important role in the deactivation and bioactivation of many environmental carcinogens including heterocyclic amines.

-It is observed that expression of NAT1 was elevated in invasive and lobular breast carcinomas when compared to normal breast tissue (2).

-It is demonstrated in MDA-MB-231 breast cancer cells line that a small molecule that inhibited NAT1 activity caused decrease cell growth and reduced ability of cancer cells to grow in soft agar. They also showed that the NAT1 inhibitor significantly reduced the invasive ability of the cells (3).

-We chose the 3 cell lines based on previously published NAT1 activity from the respective cell lines (Table 1).

Table 1-Molecular Classification of Breast Carcinoma

Breast Cancer Cell Line	Classification/ Immunoprofile	Previously Published NAT1 Activity (mmoles/min/mg protein) [4]
MDA-MB-231	Claudin-Low; Triple Negative (estrogen, progesterone, Her 2 Neu)	0.2 +/- 0.08
MCF-7	Luminal A; ER Positive	1.8 +/- 0.4
ZR-75-1	Luminal B; ER Positive	202.2 +/- 28

Methods

Cell lines- MDA-MB-231 and MCF7 cell lines were cultured in complete DMEM media (FBS, L-glutamine, and pen/strep added). ZR-75-1 cells were cultured in complete RPMI media (FBS, L-glutamine, and pen/strep added). Cells were grown at 37°C with 5% CO_2.

Construction of NAT1 Knockout Breast Cancer Cell Lines-Crisper knockout cell lines were created by transfecting plasmids coding for gRNA (guide RNAs) & GFP (Green Fluorescent Protein). We utilized 2 plasmids that target different sequences early in the NAT1 gene to generate two different clone lines (#2 and #5). An individual plasmid was transiently transfected into the cell lines then sorted with the use of Fluorescence Activated Cell Sorting (FACS). The non-fluorescent cells were not collected, while the GFP positive cells were collected and plated on $10cm^2$ plates. Afterwards, clones were isolated and grown in progressively larger plates. Once reaching 10 cm^2 plates, clones were tested for NAT1 enzyme activity. The CRISPR/CAS9 system responsible for generation of Knockout cell lines is shown below in Figure 1.
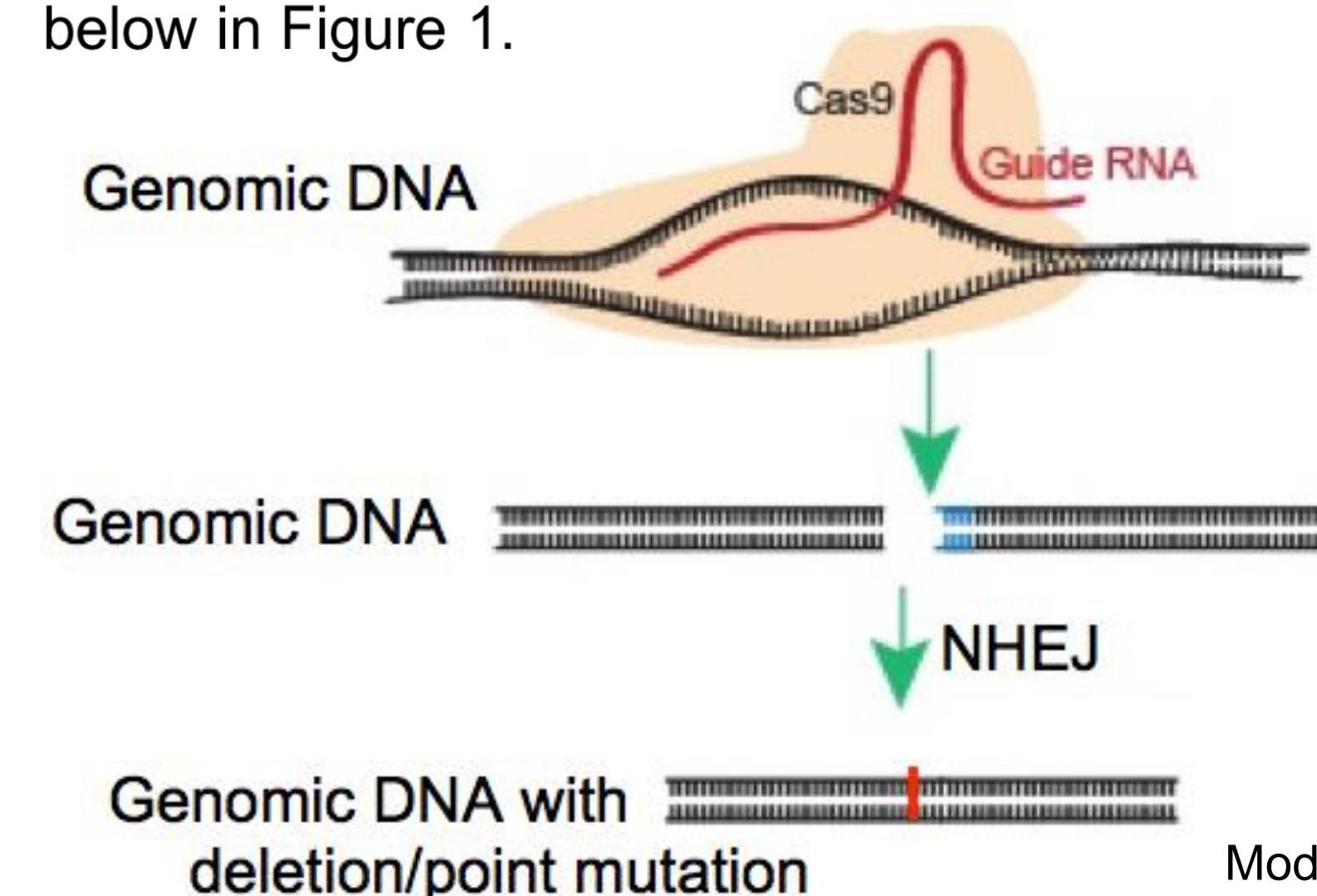

Figure 1 – CRISPR/Cas9 system uses designed guide RNA to target short unique sequences within a particular gene of interest. Guide RNA then allows Cas 9 to bind & make a double strand cut in the DNA. Then the two ends undergo non-homologous end joining (NHEJ), which is an error prone repair pathway causing possible base deletions. These deletions then lead to frame shifts/stop codons.

Modified from www.appliedstemcell.com

Determination of Doubling Time of Cell lines- Twenty five thousand cells (for MDA-MB-231 and MCF7) and fifty thousand cells (for ZR-75-1) were plated in triplicate wells for each day in 6-well plates and allowed to grow for 6 consecutive days. The cell lines were counted on day 2, 3, 4, 5, 6, and 7 after plating. The number of cells per well were determined every 24 hours. Cells were counted using a Beckman Coulter Cell Counter. The doubling time was calculated by taking the Log (current day cell number)- Log (previous day cell number) x 3.32/ time difference (T2-T1) in hours. Then the inverse of this is the doubling time.

$$\frac{1}{Doubling\ Time} = \frac{Log(current\ day\ cell\ number) - Log(previous\ day\ cell\ number) * 3.32}{Time\ Difference\ (T2 - T1)}$$

This was done for each successive day.

PABA NAT1 Activity Assay- NAT1 activity was measured in the constructed cell lines after cells were harvested from the plate. The cells were then lysed in 200 μL buffer containing 20 mM sodium phosphate, 1 mM EDTA, 0.2% triton X-100 pH 7.4 1 mM DTT and 100 μM PMSF, 1 μg/ml aprotinin and 2 μM pepstatin A. Cell lysate were then centrifuged at 15000 X g for 10 minutes and supernatant was saved for NAT1 activity assays. In vitro assays using the NAT1 selective substrate para-aminobenzoic acid (PABA) were conducted and acetylated products were separated and quantitated. Briefly, reactions (total volume 100 μL) containing 50 μL diluted cell lysate, PABA (300 μM) and acetyl coenzyme A (1 mM) were incubated at 37°C for 10 minutes. Reactions were terminated by the addition of 1/10 volume of 1 M acetic acid, and centrifuged at 15000 X g for 10 min. Supernatant was injected onto a reverse phase C18 column. Reactants and products were eluted and quantitated using a Beckman System Gold high performance liquid chromatography (HPLC) system. HPLC separation of N-acetyl-PABA was achieved using a gradient of 96:4 sodium perchlorate pH 2.5:acetonitrile at 280 nm.

Results

Effects of Arylamine *N*-acetyltransferase 1 Knockout by CRISPR/Cas 9 on Doubling Time in MDA-MB-231, MCF-7, and ZR-75-1 Breast Cancer Cell Lines
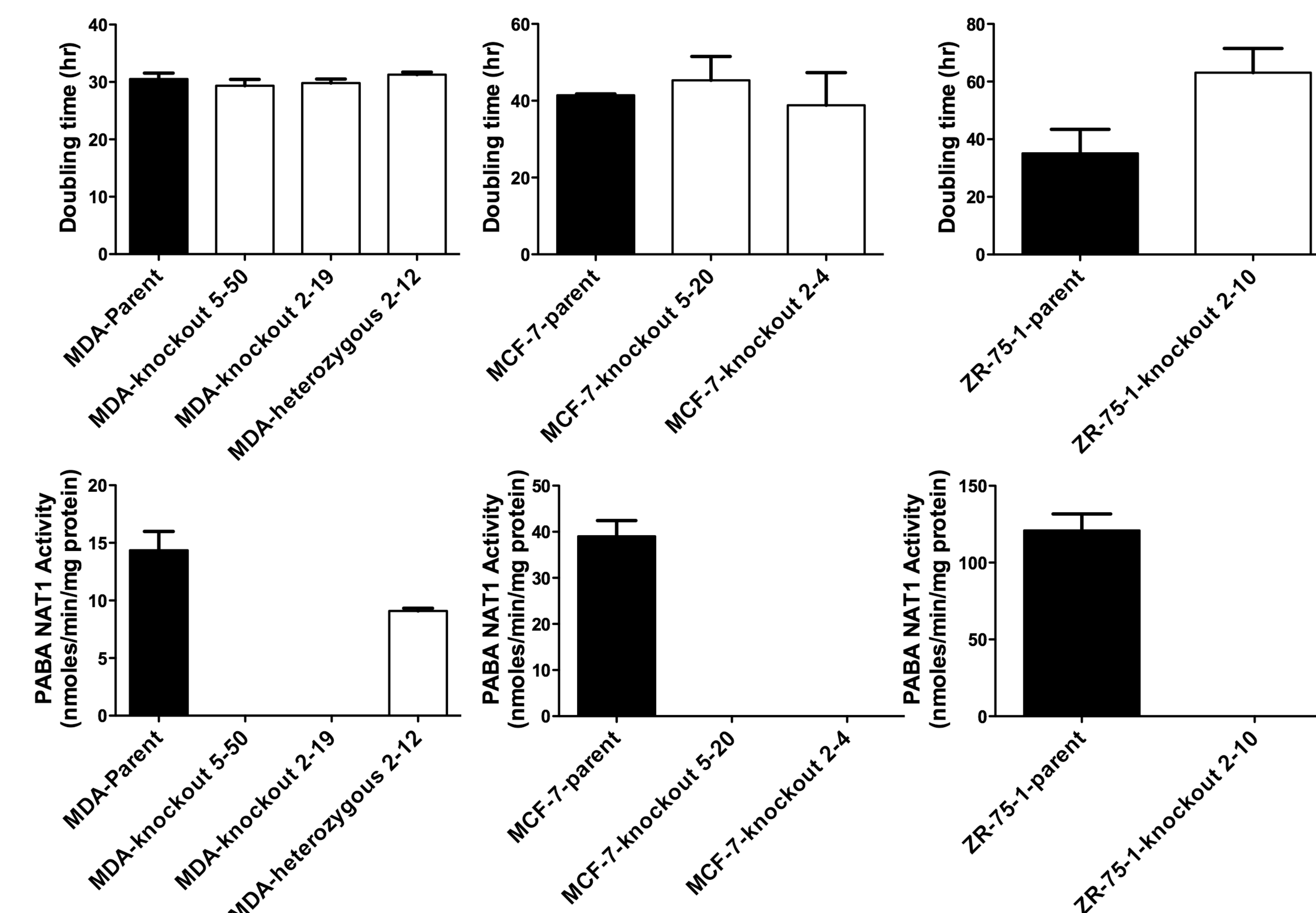
Top Row- Doubling time of MDA-MB-231, MCF-7, and ZR-75-1 breast cell lines. A One way ANOVA was run to determine whether there was difference in doubling times between MDA-MB-231, and MCF-7 cell lines p=0.4647, and 0.7579 respectively. A student t-test was run between ZR-75-1 cell lines to determine if there was a difference in doubling time with a p=0.0765. For all 3 graphs, N=3. Bottom Row- PABA NAT1 Activity in MDA-MB-231, MCF-7, and ZR-75-1 parent and knockout breast cell lines. For all three graphs, N=3. The term Knockout refers to NAT1 enzyme being eliminated. In MDA 5-50, the 5 is the guide RNA number and the 50 is the clone number. This holds for each respective cell line.

Conclusions

☐ Human NAT1 activity in breast cancer cell lines varies as MDA-MB-231 < MCF-7 <<< ZR-75-1.
☐ CRISPR/Cas 9 is very effective for NAT1 knockout in breast cancer cell lines
☐ Significant changes in doubling time in the MDA-MB-231 or MCF-7 knockout clones relative to the parent cell line were not observed.
☐ The ZR-75-1 NAT1 knockout cell line showed nearly a 2-fold increase in doubling time compared to the parent, but this did not reach statistical significant perhaps due to small sample size.
☐ Since the ZR-75-1 breast cancer cell line has the highest NAT1 activity compared to other cell lines, our results suggest the effect of NAT1 knockout on doubling time is more pronounced in breast cancer cells with high levels of NAT1 activity.
☐ Further investigations are needed to confirm this hypothesis.

Acknowledgements/References

References:
1. Siegel, R.L., K.D. Miller, and A. Jemal, *Cancer Statistics, 2015*. CA Cancer J. Clin, 2015. 65(1): p. 5-29
2. Adam, P.J.,et al., *Arylamine N-acetyltransferase-1 is highly expressed in breast cancers and conveys growth and resistance to etoposide in vitro*. Mol Cancer Res, 2003. 1(11): p. 826-35
3. Tiang, J.M., N.J. Butcher, and R.F. Minchin, *Small molecule inhibition of arylamine N-acetyltransferase Type I inhibits proliferation and invasiveness of MDA-MB-231 breast cancer cells*. Biochem Biophys Res Commun. 2010. 393(1): p95-100
4. Wakefield, L., et al. *Arylamine N-acetyltransferase 1 expression in breast cancer cell lines: a potential marker in estrogen receptor-positive tumors*. Genes Chromosomes Cancer, 2008. 47(2): p.118-26